https://doi.org/10.5194/gchron-2020-30
Preprint. Discussion started: 13 October 2020

GEOCHRONOLOGY Discussions Open Access EGU

Eruptive history and $^{40}Ar/^{39}Ar$ geochronology of the Milos volcanic field, Greece

Xiaolong Zhou[1], Klaudia Kuiper[1], Jan Wijbrans[1], Katharina Boehm1, Pieter Vroon[1]

[1]Department of Earth Sciences, VU University Amsterdam, De Boelelaan 1085, 1081 HV Amsterdam, The Netherlands.

Correspondence to: Xiaolong Zhou (z.x.l.zhou@vu.nl)

Abstract. High-resolution geochronology is essential to determine the growth-rate of volcanoes, which is one of the key factors to establish the periodicity of explosive volcanic eruptions. However, there are less high-resolution eruptive histories (>10^6 years) determined for long-lived submarine arc volcanic complexes than for subaerial complexes, since the submarine volcanoes are far more difficult to observe than subaerial ones. In this study, high-resolution geochronology and major element data are presented for Milos Volcanic Field (VF) in the South Aegean Volcanic Arc, Greece. The Milos VF has been active for over 3 Myrs, and the first two million years of its eruptive history occurred in a submarine setting that has emerged above sea level nowadays. The long submarine volcanic history of the Milos VF makes it an excellent natural laboratory to study the growth-rate of a long-lived submarine arc volcanic complex. This study reports twenty-one new high-precision $^{40}Ar/^{39}Ar$ ages and major element compositions for eleven volcanic units of the Milos VF. This allows us to refine the volcanic evolution of Milos into nine phases and five volcanic quiescence periods of longer than 200 kyrs, on the basis of age, composition, volcano type and location. Phase 1-5 (~3.34-1.60 Ma) contributed ~85% by volume to the Milos VF, whereas the volcanoes of Phase 6-9 only erupted small volumes (2-6 km^3 in DRE) rhyolitic magmas. Although there are exceptions of the felsic cone volcanoes of Phase 1-2, in general the Milos VF becomes more rhyolitic in composition from Phase 1 to Phase 9. In particular, the last three phases (Phase 7-9) only contain rhyolites. Moreover, the high-resolution geochronology suggests that there are at least three periods of different long term volumetric volcanic output rate (Q_e). In the Milos VF, the Q_e varies between 0.2 and 6.6×10^{-5} $km^3.yr^{-1}$, 2-3 orders of magnitude lower than the average for rhyolitic systems and continental arcs.

1 Introduction

Short-term eruptive histories and compositional variations of lavas and pyroclastic deposits of many arc volcanic fields are well established. However, high-resolution eruptive histories that extend back > 10^5-10^6 years have been determined only for a handful of long-lived subaerial arc volcanic complexes. Some examples are: Mount Adams (Hildreth and Lanphere, 1994), Tatara–San Pedro (Singer et al., 1997), Santorini (Druitt et al., 1999), Montserrat (Cole et al., 2002), Mount Baker (Hildreth et al., 2003a), Katmai (Hildreth et al., 2003b), and Ceboruco–San Pedro (Frey et al., 2004). In order to establish the growth rate of volcanic complexes and to disentangle the processes which are responsible for the eruption, fractionation, storage and transport of magmas over time, comprehensive geological studies are required. These include detailed field mapping, sampling, high-resolution geochronology and geochemical analysis. Based on these integrated studies, the growth-rate of volcanoes can be determined to establish the periodicity of (explosive) volcanism.

The Milos Volcanic Field (VF) is a long-lived volcanic complex which has been active for over 3 Myrs. The Milos VF erupted for a significant part of its life below sea level, similar to the other well studied volcanic structures in the eastern Mediterranean (Fytikas et al., 1986; Stewart and McPhie, 2006). The eruptive history of the Milos VF has been examined with a broad range of the chronostratigraphic techniques such as K-Ar, U-Pb, fission track, ^{14}C and biostratigraphy (e.g. Angelier et al., 1977, Fytikas et al., 1976, 1986, Traineau and Dalabakis, 1989, Matsuda et al., 1999, Stewart and McPhie, 2006, Van Hinsbergen et al., 2004 and Calvo et al., 2012). However, most of the published ages have been measured using the less precise K-Ar or

https://doi.org/10.5194/gchron-2020-30
Preprint. Discussion started: 13 October 2020

fission track methods, and modern, high precision $^{40}Ar/^{39}Ar$ ages for the Milos VF have not been published so far. In this study, (1) we provide high-precision $^{40}Ar/^{39}Ar$ geochronology of key volcanic units of the Milos VF and (2) refine the stratigraphic framework of the Milos VF with the new high-precision $^{40}Ar/^{39}Ar$ ages and major element composition. (3) We also quantify and constrain the compositional and volumetric temporal evolution of volcanic products of the Milos VF.

1.1 Geological setting

The Milos VF is part of the South Aegean Volcanic Arc (SAVA), an arc which was formed in the eastern Mediterranean by subduction of the African plate beneath the Aegean microplate (Figure 1, Nicholls, 1971; Spakman et al., 1988; Duermeijer et al., 2000; Pe-Piper and Piper, 2007; Rontogianni et al., 2011). The present-day Benioff zone is located approximately 90 km underneath the Milos VF (Hayes et al., 2018). The upper plate is influenced by extensional tectonics (e.g. McKenzie, 1978; Pe-Piper and Piper, 2013), which is evident on the island of Milos as horst and graben structures (Figure 2).

The Milos VF is exposed on the islands of the Milos archipelago: Milos, Antimilos, Kimolos and Polyegos. The focus of this study is Milos with a surface area of 151 km^2 for the main island. The geology and volcanology of Milos have been extensively studied in the last 100 years. The first geological map was produced by Sonder (1924). This work was extended by Fytikas et al. (1976) and Angelier et al. (1977) and subsequent publications by Fytikas (Fytikas et al., 1986; Fytikas, 1989). Interpretations based on volcanic facies of the complete stratigraphy were made by Stewart and McPhie (Stewart and McPhie, 2003, 2006). More detailed studies of single volcanic centres (e.g. Bombarda volcano and Fyriplaka complex) were published by Campos Venuti and Rossi (1996) and Rinaldi et al. (2003). Milos has also been extensively studied for its epithermal gold mineralization, that has been summarized by Alfieris et al. (2013). Milos was known during the Neolithic period for its export of high quality obsidian. Today the main export product is kaolinite, that is mined from hydrothermally altered felsic volcanic units in the centre of the island (e.g. Alfieris et al. 2013).

The geology of Milos can be divided into four main units: (1) metamorphic basement, (2) Neogene sedimentary rocks, (3) volcanic sequences and (4) the alluvial cover. The metamorphic basement crops out at the southwest, south and southeast of Milos (Figure 3) and is also found in many volcanic units as lithics. The metamorphic rocks include lawsonite-free jadeite eclogites, lawsonite eclogites, glaucophane schists, quartz-muscovite-chlorite and chlorite-amphibole schists (Fytikas et al., 1976, 1986; Kornprobst et al., 1979; Grasemann et al., 2018). The exposed units belong to the Cycladic Blueschist Unit (Lower Cycladic nappe), whereas eclogite pebbles in the green lahar unit are derived from the Upper Cycladic Nappe (Grasemann et al., 2018).

On top of this metamorphic basement Neogene fossiliferous marine sedimentary rocks were deposited (e.g. Van Hinsbergen et al. 2004). This sedimentary sequence can be divided into a lower unit A and upper unit B and that is unconformable overlain by volcaniclastic sediments (Van Hinsbergen et al., 2004). Unit A is 80 m thick and consists of fluviatile-lacustrine, brackish and shallow marine conglomerate, sandstone, dolomite and limestone. Unit B is 25-60 m thick and consists of a sandstone overlain by a succession of alternating marls and sapropels, suggesting a deeper marine setting (Van Hinsbergen et al., 2004). Five volcanic ash layers that contain biotite are found in this Neogene sedimentary rock sequence either suggesting that volcanic eruptions in small volume already occurred in the Milos area, or that these ash layers are derived from larger eruptions of volcanic centres further away from Milos (van Hinsbergen et al., 2004). Age determinations by bio-magneto- and cyclo-stratigraphy suggested that deposition of Unit A started at approximately 5 Ma, and that Milos subsided 900 m in 0.6 million years (Van Hinsbergen et al. 2004) due to extension. This subsidence happened ca 1.0-1.5 Myrs before the onset of the main phase of Pliocene- recent volcanism on Milos.

The Pliocene-recent volcanic sequence of Milos has been subdivided into different units by Angelier et al. (1977) and Fytikas et al. (1986). In addition, Stewart and McPhie (2006) provided a detailed facies analysis of the different volcanic units. The subdivision by Angelier et al. (1977) is not constrained well due to their limited amount of age data. The subdivision of volcanic units by Fytikas et al. (1986) and facies descriptions of Stewart and McPhie (2006) are summarized below. It is important to

https://doi.org/10.5194/gchron-2020-30
Preprint. Discussion started: 13 October 2020

note that according to Stewart and McPhie (2006), the five volcanic cycles described by Fytikas et al. (1986) are difficult to match with existing age data and the continuous progression in volcanic construction (Fig. 4). For example, the first phase of Fytikas et al. (1986), the Basal Pyroclastic Series, contains the large pumice cone-crypto dome volcanoes according to Stewart and McPhie (2006). Two of these pumice-cone crypto dome volcanoes are much younger and intercalated between the Complex of Domes and Lava Flows (CDLF) of Fytikas et al. (1986).

The first volcanic unit deposited in the Milos area is the Basal Pyroclastic Series (BPS) (Fytikas et al., 1986) or submarine felsic cryptodome-pumice cone volcanoes (Stewart and McPhie, 2006, Figure 2-4). This unit consist of thickly bedded pumice breccia with a rhyolitic-dacitic composition. These rhyolites-dacites are aphyric or contain quartz-feldspar±biotite phenocrysts. Graded sandstone and bioturbated and fossil rich (in-situ bivalve shells) mudstone are intercalated, indicating a marine environment and a water depth of several hundreds of meters (e.g. Stewart, 2003; Stewart and McPhie, 2006), whereas later degassed magmas with a similar composition intruded as sills and cryptodomes. The BPS has been strongly affected by hydrothermal fluids, especially the proximal deposits (e.g. Kilias et al., 2001).

The second volcanic unit was named the Complex of Domes and Lava Flows (CDLF, Fytikas et al., 1986) and the volcanic facies of this unit is described as the submarine dacitic and andesitic domes by Stewart and McPhie (2006). This phase of effusive submarine volcanism was predominantly andesitic/dacitic in composition and produced microcrystalline rocks with phenocrysts of pyroxene, amphibole, biotite and plagioclase. The eruption centres were mainly located along NNE faults and formed up to 300 m thick deposits extending over areas of 2.5 to 10 km around the eruption centres. In the north-eastern part of Milos, an andesitic scoria cone provided scoria lapilli and bombs to deeper water settings. Sandstone intercalated in the CDLF contains both igneous and metamorphic minerals suggesting input from the basement. Rounded pebbles of rhyolite and dacite indicate that some of the volcanic deposits were above sea level, or in very shallow, near shore environments (e.g. Stewart and McPhie, 2006).

The third volcanic unit is called the Pyroclastic Series and Lava Domes (PSLD) by Fytikas et al. (1986) and belongs to submarine-to-subaerial dacitic and andesitic lava domes of Stewart and McPhie (2006). This highly variable group is dominated by rhyolitic, dacitic and andesitic lavas, domes, pyroclastic deposits and felsic pumiceous sediments (Stewart and McPhie, 2006). Thickness varies between 50-200 m, and the deposits are located in the eastern and northern parts of Milos (Figure 2 and 3). The initial pyroclastic layers were subaqueously deposited and the extrusion of a dome resulted in deposition of talus around the margins by mass flow. On top of the dome sand- and siltstone with fossils (Ostrea fossil assemblage) and traction-current structures suggest that the top of the dome was above wave base. The youngest deposits of this unit are dacitic and andesitic lavas and domes. These domes generated subaerial block-and-ash flow and surge deposits. Paleosols within these deposits are a clear indicator that some areas were above sea level. The last unit of the PSLD is represented by large subaerial rhyolitic lava that contain quartz and biotite phenocrysts and is found near Halepa in the south-central part of Milos.

The fourth unit consists of the subaerially constructed rhyolitic Complexes of Trachilas and Fyriplaka (CTF) (Fytikas et al., 1986), which Stewart and McPhie (2006) interpreted as subaerial rhyolitic lava-pumice cones. These two volcanic complexes are built from rhyolitic pumice deposits and lavas that contain quartz and biotite phenocrysts (10-20 modal %). The deposits have a maximum thickness of 120 m and decrease to several meters thickness in the distal parts. Basement-derived schist is found as lithic clasts (Fytikas et al., 1986). In addition, the Kalamos rhyolitic lava dome that outcrops on the southern coast of Milos produced a lava that spread westwards to the Fyriplaka beach (Figure 2). This lava belongs to this fourth phase and is probably derived from an older volcano and not the Fyriplaka complex (Campos Venuti and Rossi, 1996).

The fifth volcanic unit comprises deposits from phreatic activity, especially in the northern part of the Zefiria Graben and near Agia Kiriaki (Figure 2 of Stewart and McPhie, 2006). Many overlapping craters are surrounded by lithic breccias that are composed of variably altered metamorphic basement clasts and volcanic clasts. This phreatic activity has continued into historic times (Trainau and Dalabakis, 1989). Fytikas et al. (1986) described this unit as “green lahar”, although indicated that this deposit is not a lahar but the product of phreatic eruptions in the last 0.2 Ma.

https://doi.org/10.5194/gchron-2020-30
Preprint. Discussion started: 13 October 2020

1.2 Previous geochronological studies

Previous geochronological work is summarised in Table 1. Angelier et al. (1977) reported six K-Ar ages (0.95-2.50 Ma). These ages were used in combination with field observations to divide the Milos volcanic succession into four units. However, the samples from Fyriplaka, the fourth unit, were too young to be dated by Angelier et al. (1977). Fytikas et al. (1976, 1986) published 16 K-Ar ages for Milos (0.09-3.50 Ma) including an age of 0.09-0.14 Ma for the Fyriplaka complex. Fytikas et al. (1986) also obtained 3 K-Ar ages for Antimilos (0.32 ± 0.05 Ma), Kimolos (3.34 ± 0.06 Ma) and Polyegos (2.34 ± 0.17 Ma). Trainau and Dalabakis (1989) dated the very young phreatic deposits by ^{14}C dating and found ages between 200 BC and 200 AD. Matsuda et al. (1999) published two K-Ar ages of 0.8 ± 0.1 (MI-1) and 1.2 ± 0.1 Ma (MI-4) for the Plakes dome that was also studied by Fytikas et al. (1986). Bigazzi and Radi (1981) published two fission track ages of 1.54 ± 0.18 and 1.57 ± 0.15 Ma for obsidians of Bombarda-Adamas and Demenaghaki, respectively. Later fission track studies by Arias et al. (2006) (1.57 ± 0.12 and 1.60 ± 0.06 Ma) confirmed these ages. The fission track ages are younger than the K-Ar ages given by Angelier et al. (1977; 1.84 ± 0.08 Ma for Demenaghaki) and Fytikas et al. (1986; 1.71 ± 0.05 Ma for Bombarda). In the most recent geochronological study of the Milos VF, Stewart and McPhie (2006) published 4 SHRIMP U/Pb zircon ages: Triades dacite facies (1.44 ± 0.08 and 2.18 ± 0.09 Ma), Kalogeros cryptodome (2.70 ± 0.04 Ma) and the Fylakopi Pumice Breccia (2.66 ± 0.07 Ma). All uncertainties reported here are 1 standard deviation uncertainties as reported in the original publications, except for the ^{14}C ages for which uncertainties were not specified.

2 Methods

2.1 Mineral separation and sample preparation

Samples were collected from all major volcanic units on Milos island as based on the studies of Fytikas et al. (1986), Stewart and McPhie (2006) and our own observations in the field. Photos of the sample locations and thin sections can be found in the supplementary material I. Approximately 2 kg of fresh pyroclastic material or lava was sampled from each unit. Samples were cut in ~5 cm^3 cubes using a diamond saw to remove potentially altered surfaces and obtain the fresh interior parts. These cubes were ultra-sonicated for 30 minutes in demi-water to remove dust and seawater and dried in an oven overnight at 50 °C. Dry sample cubes were crushed in a steel jaw crusher, and this fraction was split into two portions of roughly equal size. One of them was powdered in an agate shatter box and agate ball mill to a grain size of less than 2 µm for the major-element analysis. The second fraction was sieved to obtain a grain size of 250-500 µm for $^{40}Ar/^{39}Ar$ dating.

Heavy liquids density separation techniques (IJlst, 1973) were used to purify mineral separates (groundmass, biotite, amphibole) required for the $^{40}Ar/^{39}Ar$ dating. Different densities of heavy liquids were used to obtain groundmass ($2700 \leq \rho \leq 3000$ kg.m^{-3}), biotite ($2900 \leq \rho \leq 3100$ kg.m^{-3}) and/or amphibole ($\sim 3100 \leq \rho \leq 3200$ kg.m^{-3}). A Franz Isodynamic Magnet separator was used to remove the magnetic minerals from the non-magnetic minerals and groundmass. The samples for $^{40}Ar/^{39}Ar$ analysis were purified by handpicking under a binocular optical microscope to select mineral grains without visible alteration and inclusions.

2.2 $^{40}Ar/^{39}Ar$ dating

The mineral and groundmass samples were wrapped in either 6 or 9 mm aluminium foil and packed in 20 mm aluminium cups, that were vertically stacked. Based on stratigraphy and previous geochronological constraints >1 Ma samples and the <1 Ma samples were irradiated for respectively 7 and 1 hours in irradiation batches VU108 and VU110 in the CLICIT facility of the OSU TRIGA reactor. The neutron flux for all irradiations was monitored by standard bracketing using the Drachenfels sanidine (DRA; 25.52 ± 0.08 Ma, modified from Wijbrans et al., 1995 and calibrated relative to Kuiper et al., 2008) and Fish Canyon Tuff sanidine (FCs; 28.201 ± 0.023 Ma, Kuiper et al., 2008) with Min et al. (2000) decay constants.

https://doi.org/10.5194/gchron-2020-30
Preprint. Discussion started: 13 October 2020

In total 24 samples (8 groundmasses, 15 biotites and 2 amphiboles, for sample G15M0026 both biotite and amphibole were analysed) were measured by either $^{40}Ar/^{39}Ar$ fusion and/or incremental heating techniques. For incremental heating experiments 80-100 grains per sample were loaded into a 25-hole (surface per hole ~36 mm^2) copper tray together with single grain standards in ~12 mm^2 holes. The tray was prebaked in vacuum (10^{-5}-10^{-6} mbar) at 250 °C overnight to remove atmospheric argon and subsequently baked overnight at 120 °C in the ultra-high vacuum sample chamber (<5*10^{-9} mbar) and purification system connected to a Thermo Scientific Helix MC mass spectrometer.

Samples and standards are heated with a focused laser beam at 8 % power using a 50W CW CO_2 laser. The released gas was cleaned by exposure to a cold trap cooled by a Lauda cooler at -70 °C, a SAES NP10 at 400 °C, Ti sponge at 500 °C and cold SAES ST172 Fe-V-Zr sintered metal. The five isotopes of argon are measured simultaneously on five different collectors: ^{40}Ar on the H2-Faraday, ^{39}Ar on the H1-Faraday or the H1-CDD, ^{38}Ar on the AX-CDD, ^{37}Ar on the L1-CDD and ^{36}Ar on the L2-CDD for 15 cycles with 33 seconds integration time (CDD: compact discrete dynodes). The Faraday cups on H2 and H1 are equipped with 10^{13} Ohm amplifiers. Procedural blanks were measured every 2 or 3 analyses in different sequences, and air-shots were measured every 8-12 hours to correct the instrumental mass discrimination. Gain between different collectors is monitored by measuring CO_2 on mass 44 in dynamic mode on all collectors. Gain is generally stable over periods of weeks. Note, that because samples, standards and air calibration runs are measured during the same period, gain correction does not substantially change the final age results. The raw mass spectrometer data output was converted by an in-house designed Excel macro script to be compatible with the ArArCalc 2.5 data reduction software (Koppers, 2002).The atmospheric air value of 298.56 from Lee et al. (2006) is used in the calculations. The correction factors for neutron interference reactions are (2.64 ± 0.02) x10^{-4} for $(^{36}Ar/^{37}Ar)_{Ca}$, (6.73 ± 0.04) x10^{-4} for $(^{39}Ar/^{37}Ar)_{Ca}$, (1.21 ± 0.003) x10^{-2} for $(^{38}Ar/^{39}Ar)_{K}$ and (8.6 ± 0.7) x10^{-4} for $(^{40}Ar/^{39}Ar)_{K}$. All uncertainties are quoted at the 1σ level and include all analytical errors (i.e. blank, mass discrimination and neutron interference correction and analytical error in J-factor, the parameter associated with the irradiation process).

A reliable plateau age is defined as experiments with at least 3 consecutive steps overlapping at 2-sigma, containing >50% of the $^{39}Ar_{K}$, a Mean Square Weighted Deviate (MSWD) value<2.5, and with an $^{40}Ar/^{36}Ar$ inverse isochron intercept that does not deviate from atmospheric argon at 2-sigma. All the inverse isochron ages used the same steps as used in the weighted mean ages, and all relevant analytical data for the age calculations following standard practices (Schaen et al., 2020) can be found in in the supplementary material II.

2.3 Major-element analysis

Major-element concentrations were measured by X-ray fluorescence spectroscopy (XRF) on a Panalytical AxiosMax. A Panalytical Eagon2 was used to create 40mm fused glass beads of $Li_2B_4O_7/LiBO_2$ (65.5:33.5%, Johnson & Johnson Spectroflux 110) with a 1:6 dilution sample-flux ratio that were molten at 1150 °C. Sample powders were ignited at 1000 °C for 2 hours to determine loss on ignition (LOI) before mixed with the Li2B4O7/LiBO2 flux. Interference corrected spectra intensities were converted to oxide-concentrations against a calibration curve consisting of 30 international standards. The precision, expressed as the coefficient of variation (CV), is better than 0.5%. The accuracy, as measured on the international standards AGV-2, BHVO-2, BCR-2 and GSP-2 was better than 0.7% (1 RSD) (supplementary material III).

2.4 Rock textural analysis and eruption volume calculations

The crystallinity and vesicularity were estimated with Image-J software by scanning the thin section of each sample 4-6 times to cover the entire area. For the crystallinity only the phenocrysts were considered, crystals smaller than 50 μm were included in the groundmass. The estimations of crystallinity and vesicularity on the older samples (>1.0 Ma) of Milos VF are all from lava and domes. The younger samples (<1.0 Ma) are pumiceous pyroclastic units. The other old pumices of the Profitis Illias and Filakopi volcanoes are not included in this study due to the severe alteration that prevents the collection of reliable

https://doi.org/10.5194/gchron-2020-30
Preprint. Discussion started: 13 October 2020

geochemical and geochronological data on these samples. The mean value and standard deviation of the crystallinity and vesicularity were also calculated.

The minimum and/or maximum eruption volume of each volcano during each eruption period is derived from the ranges of thickness and surface areas that are reported in Campos and Rossi (1996) and Stewart and McPhie (2006). We converted these volumes to Dense Rock Equivalent (DRE) based on the magma type of different deposits. This analysis only includes the onshore deposits and results in a smaller estimate for larger pyroclastic volumes. The DRE volume is calculated using the equation of (Crosweller et al., 2012):

$$DRE\ (km^3) = \frac{tephra\ vol\ (km^3) \times tephra density\ (kg/m^3)}{magma\ density\ (kg/m^3)}$$

Tephra density is assumed to be 1000 kg/m^3 (Crosweller et al., 2012). Magma density varies depending on the magma type. Here we used 2300 kg/m^3 for rocks with a SiO_2 range of 65-77 wt.% and 2500 kg/m^3 for all samples with SiO_2 < 65 wt.% (Table 4 for major-element composition). DRE corresponds to the unvesiculated erupted magma volume and DRE volumes are converted to include vesicularity. Therefore, we did not convert the volume of some cryptodome and lavas from Profitis Illias (G15M0017), Triades (G15M0021-24), Dhemeneghaki (G15M0032B) and Halepa (G15M0013) to the DRE since they contain less than 5% vesicles.

3 Results

3.1 40Ar/39Ar age results

In this section, we present our groundmass, biotite and amphibole $^{40}Ar/^{39}Ar$ results for eleven volcanic units of Milos. The $^{40}Ar/^{39}Ar$ ages range from 0.06 to 4.10 Ma and cover most of the major volcanic units of Milos. Table 2 and 3 show the $^{40}Ar/^{39}Ar$ results of incremental heating steps and single grain fusion analyses, respectively. Note that the Irr-ID column in these two Tables represents the irradiation ID of the analytical experiment (e.g. VU108-, VU110-) and the top right superscripts (G, B, A, O) in the sample IDs (e.g., G15M0029^G, G15M0021^B) refer to groundmass, biotite, amphibole and obsidian.

3.1.1 Groundmass $^{40}Ar/^{39}Ar$ plateau and/or isochron ages

All groundmass samples yielding $^{40}Ar/^{39}Ar$ plateau and isochron ages with more than 50% $^{39}Ar_K$ and less than 2.5 MSWD included in their age spectrum are shown in Figure 4 and reported in Table 2. The $^{40}Ar/^{36}Ar$ isochron intercepts do not deviate from atmospheric argon at the 2-sigma level, unless stated otherwise (Table 3). Sample G15M0016 was collected from an extrusive dyke at Kleftiko in the southwest of Milos (Figure 2). Three incremental heating experiments were performed on the groundmass of this sample (Figure 5A). The first experiment (VU108-Z8a) produced a weighted mean age of 2.71 ± 0.02 Ma (MSWD 2.31; $^{39}Ar_K$ 79.6%; inverse isochron age 2.65 ± 0.10 Ma). The other two, VU108-Z8a_4 and VU108-Z8b_1, have plateau ages of 2.61 ± 0.03 Ma (MSWD 0.93; $^{39}Ar_K$ 57.4%; inverse isochron age 2.69 ± 0.10 Ma) and 2.67 ± 0.01 Ma (MSWD 1.50; $^{39}Ar_K$ 65.57%; inverse isochron age 2.55 ± 0.05 Ma), respectively. The three experiments are remarkably similar. Although the amount of radiogenic ^{40}Ar is low (<20%), a combined age of 2.66 ± 0.01 Ma is considered to be best estimate with a relatively high MSWD value (2.51).

Two lava samples, G15M0019 and G15M0020, were collected from Kontaro in north-eastern Milos (Figure 2). Three replicate incremental heating steps experiments of groundmass from sample G15M0019 (VU108-Z6a_4; VU108-Z6a_5 and VU108-Z6b_1, Figure 5B) were performed that are not reproducible. Their plateau ages range from 1.55 Ma to 1.62 Ma with relatively high MSWD (3.8-4.5), 56-95% of the total $^{39}Ar_K$, 34-53% of radiogenic ^{40}Ar, 0.88-1.02 of K/Ca and an atmospheric isochron intercept of 297-315. We consider the isochron age from the last experiment (VU108-Z6b_1) as the only reliable age (1.48 ± 0.02 Ma, MSWD 0.44) because of the least scatter in this experiment, and therefore the best estimate for the eruption age. Three replicate incremental heating steps experiments of groundmass from sample G15M0020 (VU108-Z5a_5; VU108-Z5b_1

https://doi.org/10.5194/gchron-2020-30
Preprint. Discussion started: 13 October 2020

and VU108-Z5b_2, Figure 5C) were analysed. These experiments are similar at the lower temperature heating steps. They produced statistically meaningful plateau ages ranging from 1.52-1.56 Ma with 41-62% of the total $^{39}Ar_K$, 18-48% of radiogenic ^{40}Ar, 1.51-1.73 of K/Ca and an atmospheric isochron intercept of 295-300. Their combined weighted mean age is 1.54 ± 0.01 Ma (MSWD 3.06; $^{39}Ar_K$ 57.32%) with 25.31% of $^{40}Ar^*$.

Sample G15M0032B (obsidian) was collected from a pumice cone volcano at Demeneghaki (Figure 2). One incremental heating experiment of this sample (VU108-Z18, Figure 5D) yielded a plateau age of 1.825 ± 0.002 Ma (MSWD 0.91; $^{39}Ar_K$ 98.6%). The $^{40}Ar^*$ is 93.86%. The inverse isochron age is identical to the weighted mean plateau age 1.825 ± 0.002 Ma. The age of 1.825 ± 0.002 Ma is considered the best estimate for the eruption age of the Demeneghaki obsidian.

3.1.2 Groundmass $^{40}Ar/^{39}Ar$ plateau and/or isochron ages (25-40% $^{39}Ar_K$ released)

The results shown in Figure 5 did not yield weighted mean plateau according to standard criteria including $^{39}Ar_K$ > 50%, but still provide some useful age information. Sample G15M0017 was collected from a cryptodome of the Profitis Illias volcano of southwestern Milos (Figure 2). Three replicate incremental heating experiments, VU108-Z7a, VU108-Z7a_4 and VU108-Z7b_1, have been performed on this sample which resulted in disturbed age spectra (Figure 6A). The consecutive lower temperature steps of all experiments define ages of <2.5 Ma, which is much younger than the ages of the submarine pyroclastic products of the lower series at Kleftiko and/or Profitis Illias (3.0-3.5 Ma, Fytikas et al., 1986 and Stewart and McPhie, 2006). At the consecutive higher temperature heating steps, these experiments yielded 3.64 ± 0.08 Ma ($^{40}Ar/^{36}Ar$ 293.87 ± 4.77; VU108-Z7a), 4.10 ± 0.06 Ma ($^{40}Ar/^{36}Ar$ 298.44 ± 15.51; VU108-Z7a_4) and 3.41 ± 0.05 Ma ($^{40}Ar/^{36}Ar$ 295.97 ± 7.34; VU108-Z7b_1). The total fusion and inverse isochron ages of the three experiments gave large ranges of 2.25-3.23 and 3.68-4.14 Ma, respectively, and none of these high temperature heating steps produced a statistical plateau (all MSWD > 2.0). The amount of radiogenic ^{40}Ar of both $^{40}Ar/^{39}Ar$ result from our sample and K-Ar from previous studies (Fytikas et al., 1986) is rather low (<15%) for a sample of this age based on our laboratory experience. Therefore, the estimated age range for the oldest volcanic products of the Milos VF should be confirmed by other dating techniques.

Sample G15M0015 is also a cryptodome breccia from Profitis Illias (Figure 2). Two replicate incremental step heating experiments were performed on the groundmass of this sample (VU108-Z9a and VU108-Z9b_1, Figure 6B). Experiment VU108-Z9a groundmass shows a disturbed age spectrum with ages increasing from ~3 Ma in the initial heating steps to ~3.2 Ma followed by a decrease to ~3 Ma in the high temperature heating steps. The consecutive heating steps only exist at the lower temperature steps yielding a "plateau" of 3.12 ± 0.02 Ma (MSWD 9.07). Due to the excess argon ($^{40}Ar/^{36}Ar$ 304.19 ± 1.25 comprising 43.07% of the released $^{39}Ar_K$), the inverse isochron of 3.06 ± 0.02 Ma (MSWD 0.01) is more reliable for this analysis. The inverse isochron age of the second groundmass (VU108-Z9b_1) is identical at 3.04 ± 0.02 Ma (MSWD 1.14; $^{39}Ar_K$ 27.00%) and $^{40}Ar/^{36}Ar$ of 293.83 ± 1.38 obtained at high temperature steps. The two experiments are remarkably similar. Although the sample does not formally fulfil the definition of a plateau age comprising >50% $^{39}Ar_K$ released, a combined age of 3.06 ± 0.02 Ma (MSWD 1.14; $^{39}Ar_K$ 22.79%, $^{40}Ar^*$ 41.77%) most likely represents the eruption age. This $^{40}Ar/^{36}Ar$ age is consistent with the K-Ar age from the same lithology of 3.08 ± 0.08 Ma (Fytikas et al. 1986).

Sample G15M0029 is an andesite collected from Korakia in the northeast of Milos (Figure 2). Two incremental heating experiments (VU108-Z16a and VU108-Z16b_1, Figure 6C) were performed on this sample. The two experiments are remarkably similar with a decreasing age from ~2.85 Ma at the lower temperature heating steps to 2.65 Ma at the higher temperatures. The higher temperature heating steps of both experiments yielded weighted mean plateau ages of 2.67 ± 0.01 Ma (MSWD 0.96; $^{39}Ar_K$ 23.61%, $^{40}Ar^*$ 56.34%; inverse isochron age 2.68 ± 0.02 Ma) and 2.69 ± 0.01 Ma (MSWD 1.32; $^{39}Ar_K$ 27.08%, $^{40}Ar^*$ 55.78%; inverse isochron age 2.67 ± 0.03 Ma). The isochron intercepts for both experiments are atmospheric. The combined age of 2.68 ± 0.01 Ma should be considered with caution due to the rather low amount of released ^{39}Ar (23-28%).

https://doi.org/10.5194/gchron-2020-30
Preprint. Discussion started: 13 October 2020

283 **3.1.3 Single biotite grain $^{40}Ar/^{39}Ar$ fusion and/or isochron ages**

284 Results of nine single fusion experiments are given in Figure 7. Nine or ten replicate single fusion experiments were conducted
285 on 5-10 grains biotite per fusion. Sample G15M0006 is from a solid in-situ dacite with columnar joints from the Kalogeros
286 cryptodome in the northeast of Milos (VU108-Z11, Figure 7A). The sample shows a weighted mean age of 2.72 ± 0.01 Ma
287 with 9 out of 10 total fusion experiments (MSWD 1.95; 9/10) with an average 47.9% of radiogenic ^{40}Ar. The inverse isochron
288 age is 2.62 ± 0.04 Ma (MSWD 0.99). Note that excess argon ($^{40}Ar/^{36}Ar$ 310.2 ± 4.0) is present, hence the inverse isochron age
289 is younger compared to the weighted mean age. The isochron age of 2.62 ± 0.04 Ma is considered as the best estimate for the
290 emplacement age.
291 Sample G15M0025 was collected from the Mavros Kavos lava dome located in the west of Milos (Figure 2). The biotite of
292 this sample (VU108-Z2, Figure 7B) shows a weighted mean age of 2.36 ± 0.01 Ma (MSWD 0.70; 9/10; $^{40}Ar^*$ 37.60%, inverse
293 isochron age 2.34 ± 0.04 Ma) with an $^{40}Ar/^{36}Ar$ intercept of 300.6 ± 3.5. The age of 2.36 ± 0.01 Ma is considered the best
294 eruption age estimate for this sample.
295 Sample G15M0023 and -24 are from the Triades lava dome of the northeast of Milos (Figure 2). A mafic enclave G15M0022
296 (host rock G15M0021) was collected from a lava near Cape Vani (Figure 2). The total fusion experiments of the biotites show
297 that their initial $^{40}Ar/^{36}Ar$ estimates overlap with air (296-300). The total fusion ages gave the best estimates for their eruption
298 ages of 2.10-2.13 Ma using 22 out of 31 fusions with a range of radiogenic ^{40}Ar between 30-36% (Figure 7B).
299 Sample G15M0013 is from the rhyolitic Halepa lava dome in the south of Milos (Figure 2). The total fusion experiment
300 (VU108-Z13, Figure 7C) on biotite of this sample produced a weighted mean age of 1.04 ± 0.01 Ma (MSWD 1.62; 9/10, $^{40}Ar^*$
301 26.3%; inverse isochron age 1.02 ± 0.04 Ma) with an initial $^{40}Ar/^{36}Ar$ estimate of 299. 8 ± 4.1. The best estimate for the
302 eruption age of the Halepa rhyolite is 1.04 ± 0.01 Ma.
303 Sample G15M0034 and 35 were collected from a lava dome located southeast of the Trachilas cone (Figure 2). Nine total
304 fusion experiments (VU108-Z21, Figure 7C) were performed on biotite of sample G15M0035 and yielded 0.63 ± 0.02 Ma
305 (MSWD 1.26; 6/9; $^{40}Ar^*$ 4.9%; inverse isochron age 0.77 ± 0.13 Ma). The atmospheric isochron intercept overlaps with air at
306 2-sigma (296.4 ± 1.7). The 4.9% of radiogenic ^{40}Ar is so low that we should consider the age of 0.63 ± 0.02 Ma with caution.
307 For biotite of sample G15M0034 (VU108-Z20, Figure 7C) one total fusion experiment produced a weighted mean age of 0.51
308 ± 0.02 Ma (MSWD 0.95; 6/10; $^{40}Ar^*$ 3.5%; inverse isochron age 0.61 ± 0.08 Ma) with an atmospheric isochron intercept. The
309 age of 0.51 ± 0.02 Ma also needs to be considered as possibly suspect due to the low amount of radiogenic ^{40}Ar.
310 Sample G15M0033 was collected from the Kalamos lava along the coast of the southwest of the Fyriplaka rhyolitic complex
311 (Figure 2). Biotite of this sample (VU108-Z19, Figure 7C) yielded 0.412 ± 0.004 Ma (MSWD 1.10; 8/10; inverse isochron
312 age 0.39 ± 0.02 Ma) with ~22.2% of radiogenic ^{40}Ar which is considered as the eruption age for the Kalamos lava.

313 **3.1.4 Multiple biotite grain $^{40}Ar/^{39}Ar$ incremental heating plateau and/or isochron ages**

314 Figure 8 displays the biotite $^{40}Ar/^{39}Ar$ ages measured by the incremental heating steps method. Sample G15M0021 is the host
315 lava of mafic enclave G15M0022. Twelve replicate total fusion experiments of its biotite (VU110-Z4, Table 3) produced an
316 age of 2.48 ± 0.04 Ma (MSWD 1.49; 4/12, $^{40}Ar^*$ 36.09%; inverse isochron age 3.44 ± 0.46 Ma). Although this suggests a
317 correct age, the large analytical error of each fusion (>0.3 Ma on average) and poor reproducibility (4/12) of this experiment
318 probably results in an unreliable age. Therefore, two more incremental heating experiments were performed on this sample
319 (VU110-Z4_2 and VU110-Z4_2b, Figure 8A), that gave an age of 1.97 ± 0.01 Ma (MSWD 1.66; $^{39}Ar_K$ 63.8%, $^{40}Ar^*$ 54.7%;
320 inverse isochron age 1.97 ± 0.03 Ma) and 2.01 ± 0.01 Ma (MSWD 6.76; $^{39}Ar_K$ 75.39%, $^{40}Ar^*$ 57.84%; inverse isochron age
321 2.04 ± 0.05 Ma), respectively. The scatter in the latter is too high to define a reliable plateau age and the first incremental
322 heating experiment is considered as the best estimate of the eruption age of this sample.
323 Sample G15M0007 was collected from the rhyolitic Trahilas complex in the north of Milos (Figure 2). Twenty-two total fusion
324 (VU110-Z12, Table 3) and two incremental heating experiments (VU110-Z12a and 12b, Figure 8B) were performed on biotite

https://doi.org/10.5194/gchron-2020-30
Preprint. Discussion started: 13 October 2020

of this sample. The total fusion experiments did not result in a reliable age due to the large errors of single steps (± 0.19 Ma on average) and the rather low amount of radiogenic ^{40}Ar (9.1%). On the other hand, the first incremental heating experiment produced a plateau age of 0.30 ± 0.01 Ma (MSWD 4.61; $^{39}Ar_K$ 56.60%; inverse isochron age 0.28 ± 0.05 Ma) including 14.51% of radiogenic ^{40}Ar. The second incremental heating experiment yielded a plateau of 0.317 ± 0.004 Ma (MSWD 1.29; $^{39}Ar_K$ 74.05%; inverse isochron age 0.31 ± 0.03 Ma) with a higher amount of radiogenic ^{40}Ar (18.30%). The isochron intercepts of both incremental heating experiments are atmospheric. The second experiment is the best estimate for the eruption age, since it contained the largest amount of radiogenic ^{40}Ar and has a better reproducibility of single heating steps.

Three pumice clasts (G15M0008-9 and G15M0012) were sampled from different layers of the Fyriplaka complex (Figure 2). The first incremental step heating experiment of biotite from sample G15M0009 (VU110-Z23a, Figure 8C) gave negative ages at the lower temperature heating steps. Four consecutive higher temperature heating steps seem to define a "plateau" of 0.11 ± 0.02 Ma (MSWD 1.37) only using 18.33% of the total $^{39}Ar_K$ with 1.65% of radiogenic ^{40}Ar. The second experiment (VU110-Z23b) also yielded a "plateau" of 0.11 ± 0.03 Ma (MSWD 6.77) at higher temperature heating steps including 41.05% of the total $^{39}Ar_K$ and 3.13% of radiogenic ^{40}Ar. The significantly larger error of the isochron age may be due to the clustering of data close to zero on the y-axis. The two experiments (VU110-Z23a and Z23b) are comparable. The combined age of 0.11 ± 0.02 (MSWD 3.5) is consistent with the age of 0.09-0.14 Ma from Fytikas et al. (1986). Although only 29.50% of the released $^{39}Ar_K$ was used for this sample, we believe this age is the eruption age of this layer in the Fyriplaka complex.

For biotite of sample G15M0012 both incremental step heating experiments are comparable. Both of them yielded plateau ages of 0.05 ± 0.01 Ma (VU110-Z24a; MSWD 3.09; $^{39}Ar_K$ 38.89%, $^{40}Ar^*$ 2.89%; inverse isochron age 0.14 ± 0.03 Ma) and 0.09 ± 0.02 Ma (VU110-Z24b; MSWD 8.16; $^{39}Ar_K$ 48.04%, $^{40}Ar^*$ 4.59%; inverse isochron age 0.09 ± 0.05 Ma) at higher temperature heating steps (Figure 8C). The clustering of data points of experiment VU110-Z24a could result in the lower initial estimate of $^{40}Ar/^{36}Ar$ (285.98 ± 4.76). However, the combined age of 0.07 ± 0.01 Ma, using 43.53% of the total $^{39}Ar_K$ with an atmospheric isochron intercept (295.67 ± 7.39), could be the representative age of eruption.

Biotite of sample G15M0008 did not result in a reliable plateau in the first incremental step heating experiment (VU110-Z22a, Figure 8C) but shows a very disturbed age spectrum. The second experiment (VU110-Z22b) yielded 0.062 ± 0.003 Ma (MSWD 0.91) using 71.81% of the total $^{39}Ar_K$ with 2.69% of radiogenic ^{40}Ar as the best estimate of the eruption age.

3.1.5 Multiple amphibole grain $^{40}Ar/^{39}Ar$ multi-grain incremental heating plateau and/or isochron ages

There are only two amphibole samples that yielded $^{40}Ar/^{36}Ar$ plateau and/or isochron ages (Figure 9A and B). Sample G15M0004 was collected from the pyroclastic series of Adamas from the PSLD (Fytikas et al., 1986), to the north of Bombarda (Figure 2). Two replicate heating experiments of G15M0004 amphibole (VU108-Z10_1 and VU108-Z10_2) were performed yielding 2.99 ± 0.11 Ma (MSWD 1.00; $^{39}Ar_K$ 87.31%, $^{40}Ar^*$ 16.36%; inverse isochron age 7.89 ± 2.46 Ma) and 2.86 ± 0.09 Ma (MSWD 1.50; $^{39}Ar_K$ 86.18%, $^{40}Ar^*$ 17.58%; inverse isochron age 0.70 ± 0.29 Ma). The variable atmospheric isochron intercept of both experiments ($^{40}Ar/^{36}Ar$ 202.39 ± 48.47 and 348.91 ± 27.33) is due to clustering of the data points. Note that also the amount of radiogenic ^{40}Ar is rather low (~17%). The two experiments are remarkably similar. A combined inverse isochron age of 1.95 ± 0.45 Ma (MSWD 1.17; $^{40}Ar/^{36}Ar$ 319.51 ± 14.70) is considered the best estimate, but ideally this age should be checked by other techniques.

Sample G15M0026 is from the same location as sample G15M0025, which gives us the opportunity to compare the biotite age with the amphibole age. One total fusion experiment of biotite (VU108-Z1b) yielded a weighted mean age of 2.35 ± 0.01 Ma (MSWD 1.36; $^{40}Ar^*$ 38.6%). The atmospheric isochron intercept is low ($^{40}Ar/^{36}Ar$ 292.01 ± 2.92), the inverse isochron age of 2.42 ± 0.04 Ma (MSWD 0.93) is considered the best result from the biotite. Two incremental heating experiments for amphibole (VU108-Z1b_1 and VU108-Z1b_2) gave plateau ages of 2.67-2.70 Ma which are much higher values than the biotite inverse isochron ages (2.28-2.31 Ma). This result could be caused by the high $^{40}Ar/^{36}Ar$ isochron intercepts (>320) with large uncertainties of ~29. Therefore, on the basis of the remarkable similarity of the two experiments, the combined inverse

https://doi.org/10.5194/gchron-2020-30
Preprint. Discussion started: 13 October 2020

isochron age of 2.31 ± 0.28 Ma (MSWD 0.93, $^{39}Ar_K$ 71.36%, $^{40}Ar^*$ 34.97%) is considered as the best estimate from amphibole which overlaps with the biotite age of 2.42 ± 0.03 Ma. This biotite age of 2.42 ± 0.03 Ma is considered to the best approximation of the eruption age.

3.2 Major element results

Major-element results are given in Table 4. The major element compositions range from 54 to 78 wt.% SiO_2 (basaltic-andesite-rhyolite to dacite-rhyolite, see Figure 10A). The most felsic samples (SiO_2>75 wt.%) belong to the Fyriplaka and Trachilas complexes. Our data overlap with those of previous studies and display a similar range in SiO_2-K_2O (Francalanci and Zellmer, 2019 and reference therein). The samples of Polyegos are similar to the Fyriplaka and Trachilas complexes, whereas the older Milos samples overlap with Kimolos and Antimilos (Fytikas et al., 1986, Francalanci et al., 2007).
Although some samples of Antimilos are tholeiitic, all of the Milos volcanic units belong to the calc-alkaline and medium to high-K series (Figure 10B). A mafic inclusion, sample G15M0022, has high K_2O (6%), similar to sample G15M0021 (7.2 wt.%). Both of them were collected from the Vani Cape area (Fig. 2). The SiO_2 wt.% versus our $^{40}Ar/^{39}Ar$ ages diagram (Figure 11A) shows that there is a tendency of the volcanic units to become more felsic over time. In the diagram with K_2O/SiO_2 versus age there is no significant change (Figure 11B).

3.3 Variations of rock texture and eruption volume with ages

Figure 11C and D show the variations of crystallinity and vesicularity of the studied samples versus the $^{40}Ar/^{39}Ar$ ages. Apart from the pumiceous pyroclastic units, Trachilas and Fyriplaka complexes (<1.0 Ma), Profitis Illias (>3.0 Ma) and Filakopi (~2.66 Ma) volcanoes the vesicularity (0.1-10%) and crystallinity (10-40%) tends to become higher with younger deposits. The volcanic complex of Milos was largely (~85% by volume) constructed before ~1.6 Ma (Figure 12). During 1.59-0.06 Ma, only a small volume (~15%) of rhyolitic magma was added from different eruption vents. The ratio of eruption volume of Milos VF in submarine to subaerial is 6-8. At least approximately 12 km^3 in DRE (minimum) has been added by submarine volcanism, whereas ~2 km^3 was subaerially added.

4 Discussion

In this section, our $^{40}Ar/^{39}Ar$ results are compared with previously published geochronological data, and subsequently used to refine the stratigraphy of the Milos VF. In the last part, we will discuss the temporal variations in major elements and the volumetric volcanic output rate of the Milos VF.

4.1 Comparison with the previous geochronological studies on the Milos VF

K-Ar ages may show undesirable and unresolvable scatter due to various problems: (1) in accurate determination of radiogenic argon due to either incorporation of excess argon or incomplete degassing of argon during the experiments; (2) inclusion of cumulate or wall rock phenocrysts in bulk analyses; (3) disturbance of a variety of geological processes such as slow cooling, thermal reheating; (4) unrecognized heterogeneities due to separate measurements of potassium and argon content by different methods; (5) requirement of relatively large quantities (milligrams) of pure sample (e.g. Lee, 2015). In addition to these methodological issues, in the case of Milos we observe that hydrothermal alteration caused substantial kaolinitisation, in particular the felsic volcanic samples, that most likely has affected the K-Ar systematics. Some of these issues are also valid for the $^{40}Ar/^{39}Ar$ method, however, the K-Ar method does not allow testing if ages are compromised.
$^{40}Ar/^{39}Ar$ ages only need isotopes of argon to be measured from a single aliquot of sample with the same equipment that can eliminate some of the problems with sample inhomogeneity. Furthermore, step heating and multiple single fusion experiments can shed light on sample inhomogeneity due to partial alteration effects. The high sensitivity of modern noble gas mass

https://doi.org/10.5194/gchron-2020-30
Preprint. Discussion started: 13 October 2020

spectrometers for $^{40}Ar/^{39}Ar$ measurements results in very small sample amounts needed for analysis, that can yield more information on the thermal or alteration histories than larger samples. Moreover, other argon isotopes (^{36}Ar, ^{37}Ar and ^{38}Ar) can be used to infer some information about the chemical compositions (i.e. Ca and Cl) of samples. A high-resolution laser incremental heating method of $^{40}Ar/^{39}Ar$ dating allows us to resolve the admixture of phenocryst-hosted inherited ^{40}Ar in the final temperature steps of the incremental step heating experiments. More than half of our $^{40}Ar/^{39}Ar$ ages derived for this study are based on this method. All incremental step heating experiments are reproducible, except for the sample G15M0017 which gave the oldest age. The total fusion experiments of this study gave at least five times smaller analytical uncertainty (1SE on average ≤0.01 Ma) than the previous studies using conventional K-Ar (Angelier et al., 1977; Fytikas et al., 1976, 1986; Matsuda et al., 1999) and SHRIMP U/Pb zircon methods (Stewart and McPhie, 2006). Fission track dating on obsidians of the Milos VF produced two ages (Bigazzi and Radi, 1981; Arias et al., 2006) which seems to overlap with the K-Ar and $^{40}Ar/^{39}Ar$ ages, but with larger uncertainty. U/Pb zircon ages could indicate the timing of zircon formation at high temperature (>1000 °C) in magma chambers significantly prior to volcanic eruption (e.g. Flowers et al., 2005). On the other hand, the lower closure temperature of K-rich minerals (<700 °C) makes the K-Ar and $^{40}Ar/^{39}Ar$ ages better suited to determine the timing of extrusion of volcanic products (e.g. Grove and Harrison, 1996; Cassata and Renne, 2013).

The MSWD value, as a measure of the scatter of the individual step ages, is based on the error enveloping around the data point. The decrease in error will automatically cause an increase in MSWD (e.g. York, 1968; Wendt and Carl, 1991). The MSWD values reported in this study are relatively high. In part this is caused by the fact that modern multi-collector mass spectrometers used for $^{40}Ar/^{39}Ar$ dating can measure the isotope ratios very precisely, which in turn would result in the increase in MSWD. It will be more valuable and challenging to find a plateau or isochron age which meets the MSWD criteria (<2.5) by modern multi-collector $^{40}Ar/^{39}Ar$ dating than by K-Ar or $^{40}Ar/^{39}Ar$ dating using a single detector instrument (e.g. Mark et al., 2009).

Potential drawbacks of the $^{40}Ar/^{39}Ar$ method are its dependence on neutron irradiation causing the production of interfering argon isotopes that needs to be corrected for. The uncertainty in ages of standards that are required to quantify the neutron flux also need to be incorporated in the final ages as are uncertainties related to decay constants (supplementary material II). Finally, recoil can occur during irradiation. Minerals such as biotite can be prone to recoil, yielding slightly older ages (e.g. Hora et al., 2010).

Figure 13 compares previous published K-Ar, U/Pb zircon and fission track ages from the same volcanic units with the new $^{40}Ar/^{39}Ar$ data of this study. In general, there is a good agreement, however, six ages out of twenty-three differ significantly from previous studies that will be discussed below.

The obsidian fission track ages (Bigazzi and Radi, 1981; Arias et al., 2006) for the Dhemeneghaki volcano are 0.25 My younger than the K-Ar ages (1.84 Ma, Angelier et al., 1977) and the $^{40}Ar/^{39}Ar$ age of this study (1.825 Ma, G15M0032B). The good agreement between the K-Ar and $^{40}Ar/^{39}Ar$ ages suggests that the fission track ages record another, lower temperature event, than the K-Ar and $^{40}Ar/^{39}Ar$ ages. In addition, the larger uncertainty of fission track ages (>0.05 Ma) also overlaps with the $^{40}Ar/^{39}Ar$ age at 2-sigma. We assume that the $^{40}Ar/^{39}Ar$ age is the correct extrusion age for the obsidian of the Dhemeneghaki volcano.

Angelier et al. (1977) reported one dacite sample in the northwest of Milos with an age of 1.71 Ma (Angelier_3, location 3 on Figure 3 of Angelier et al., 1977). Argon loss could result in these ages (Angelier_3-5 in Figure 13) being younger than our $^{40}Ar/^{39}Ar$ groundmass ages of 1.97 ± 0.01 Ma (dacite sample G15M0021 and -22).

The amphibole of sample G15M0004 of the Adamas dacitic lava dome, located ~1 km north of rhyolitic Bombarda volcano, gave an inverse isochron age of 1.95 Ma ± 0.45 Ma. This age overlaps with the K-Ar age for the Adamas lava dome of 2.03 ± 0.06 Ma (dacite M 66) of Fytikas et al. (1986). The large analytical uncertainty of our sample G15M0004 is caused by a combination of low $^{40}Ar^*$ yields and clustering of data points that define the inverse isochron showing excess argon was

https://doi.org/10.5194/gchron-2020-30
Preprint. Discussion started: 13 October 2020

identified by the $^{40}Ar/^{39}Ar$ method ($^{40}Ar/^{36}Ar$ 319.51 ± 14.70), whereas the presence of excess argon cannot be tested by the K-Ar technique, implying that the Fytikas et al. (1986) might be slightly old.

The Korakia andesite has an age of 1.59 ± 0.25 Ma (M 103, Fytikas et al., 1986) and was deposited in a submarine-subaerial environment on top of the Sarakiniko Formation that was dated based on paleomagnetic polarity in combination with a K-Ar age (1.80-1.85 Ma, Stewart and McPhie, 2003 and reference therein). The much older $^{40}Ar/^{39}Ar$ groundmass age (2.68 ± 0.01 Ma) of Korakia andesite sample G15M0029 is unreliable and it could indicate the emplacement age of the Kalogeros cryptodome (2.70 ± 0.04 Ma, Stewart and McPhie, 2006) or represents a geological meaningless age with only 23-27% of the total ^{39}Ar released in the "plateau". In this case, the K-Ar age of 1.59 ± 0.25 Ma is considered as the likely eruption age for the Korakia andesite although its argon loss or excess Ar component is unknown.

We obtained $^{40}Ar/^{39}Ar$ ages of 3.41-4.10 Ma and 3.06 ± 0.02 Ma, respectively, from the groundmasses of dacite samples G15M0017 and G15M0015 in the southwest of Milos (Figure 2 and 14B). Both of them are from derived the coherent dacite facies of the rhyolitic Profitis Illias volcano based on the Figure 11 of Stewart and McPhie (2006). Sample G15M0015 yielded much higher radiogenic ^{40}Ar (41.77%) than that of sample G15M0017 (<10% of $^{40}Ar^*$), and the rhyolite sample M 164 from Fytikas et al. (1986) (23.5% of $^{40}Ar^*$) gave an estimate the eruptive age of 3.08 ± 0.08 Ma to the Profitis Illias volcano which is much younger than that given by our sample G15M0017 (Figure 13). Therefore, we considered our $^{40}Ar/^{39}Ar$ ages of 3.06 ± 0.02 Ma is the best estimate of the emplacement age of the coherent dacite facies of Profitis Illias volcano.

A basaltic andesite dyke near Kleftiko on the south-western coast of Milos has a K-Ar age of 3.50 ± 0.14 Ma which only gave 13.9% of $^{40}Ar^*$ (Fytikas et al. 1986). This age is significantly older than the eruptive ages of Profitis Illias volcano which they intrude (Stewart, 2003). Although containing relatively low $^{40}Ar^*$ (16.87%), our $^{40}Ar/^{39}Ar$ age of 2.66 ± 0.01 Ma with 67.27% of $^{40}Ar^*$ from the groundmass of basaltic andesitic sample G15M0016 of the dyke near Kleftiko is probably an accurate intrusion age.

4.2 The published ages of the other volcanic units

In order to construct a high-resolution geochronology on the Milos VF, we need to consider as many volcanic units as possible. Except for the eleven units we present, five more volcanic units can be included in the Milos VF. However, we were unable to obtain the unaltered samples of these five unites so that we could not date them. Instead, the published ages of them are shown here.

They are the Profitis Illias volcano (3.08 ± 0.08 Ma with 23.5 (%), Fytikas et al., 1986), the Mavro Vouni lava dome (2.50 ± 0.09 Ma with 55.2 $^{40}Ar^*$ (%), Anglier et al., 1977) in the south-western part of Milos, the Bombarda volcano (1.71 ± 0.05 Ma with 24.3 $^{40}Ar^*$ (%), Fytikas et al., 1986), the Plakes volcano (0.97 ± 0.06 Ma with 10.2 $^{40}Ar^*$ (%), Fytikas et al., 1986, and 0.8-1.2 Ma with 5.4-11.9 $^{40}Ar^*$ (%) Matsuda et al. 1999), and the scoria cone in the north-east. Scoria deposits are found that Stewart and McPhie (2006) attributed to an andesitic scoria cone that was submarine, and maybe occasionally above sea level. No age data for this deposit has been published so far. But its stratigraphic position is between MIL 365 (2.66 Ma, Stewart and McPhie, 2006) and M103 (1.59 Ma, Fytikas et al., 1986), which is shown in Figure 10 of Stewart and McPhie (2006). Therefore, this scoria cone was likely active in the north-eastern part of the Milos VF between 2.6-1.6 Ma.

In addition, the Sarakiniko pumice (1.85 ± 0.10 Ma with 13.6 $^{40}Ar^*$ (%), Fytikas et al., 1986) deposits eastward of Adamas (Fig. 2). This unit belongs to the reworked pyroclastic sediment of the Adamas lava dome (Rinaldi and Venuti, 2003). Therefore, the K-Ar age from Sarakiniko unit was not considered as an eruption age in this study. We did not sample the neighbouring islands of the Milos VF and also did not attempt to date the products of the recent phase of phreatic activity that Traineau and Dalabakis (1989) obtained ^{14}C ages of 200 BC and 200 AD.

https://doi.org/10.5194/gchron-2020-30
Preprint. Discussion started: 13 October 2020

4.3 Implications for the stratigraphy of the Milos VF

Figures 14 and 15 summarize our stratigraphic interpretation of the Milos VF based on our new $^{40}Ar/^{39}Ar$ ages in combination with previously published facies analysis by Stewart and McPhie (2006) and biostratigraphic, fission track, ^{14}C, K-Ar and U-Pb ages. We propose to divide the volcanic activity in the Milos VF into 9 distinct phases and 5 periods of quiescence. Here we define a "phase" as a period of the Milos VF that one type of volcano was active (e.g. pumice cone/crypto dome, lava dome, tuff cone) in a certain area of the Milos VF (NW, NE, SE or SW part) (Fig. 2 and 15). In addition, we use the chemical composition of the volcanic units as an extra distinguishing characteristic (e.g. andesite, dacite and rhyolite). The lower and upper boundary of these phases are based on the $^{40}Ar/^{39}Ar$ data of this study, in combination with previously published age data (Fig. 14). The errors of the previously published K-Ar data for volcanic units not dated in the present study result in estimates for some events that are probably longer than they in reality were. Most of the time the Milos VF was in quiescence, and there are periods during which long breaks are recoded in the stratigraphic succession. In this study we define a period of volcanic quiescence if this period is longer than 200 kyrs. We did not consider the Matsuda et al. (1999) fission track ages to define the periods for quiescence, as the fission track ages seem to be offset to other dating techniques ages obtained from the same deposits (see discussion above). Figure 15 shows that there are five periods of no, or limited volcanic activity on Milos, between phases 1-2 (Q1), 3-4 (Q2) 6-7 (Q3), 7-8 (Q4) and 8-9 (Q5). These periods are also visible in the published age data, with two above mentioned exceptions from Matsuda et al. (1999). However, this does not mean that during the periods of these volcanic quiescence no eruptions occurred the Milos VF, as in Q2 probably the Polyegos lava dome was formed, and in Q5 the domes of Antimilos were extruded (Fig. 15).

The exact start of volcanism in the Milos VF is still unclear since these older deposits are strongly hydrothermally altered. Van Hinsbergen et al. (2004) reported 5 ash layers in the Pliocene sedimentary rocks of southern Milos, ranging between 4.5-3.7 Ma in age, based on biostratigraphy, magnetostratigraphy and astronomical dating. In a slightly wider circle around Milos island, the 6.943 ± 0.005 Ma a1-tephra event recorded in several locations on nearby Crete (Rivera et al., 2011), shows that explosive volcanism along the Aegean arc, possibly on Milos, already occurred during the Messinian. These ash beds cannot be traced to currently exposed centres in the Milos VF and could conceivably be related to volcanic centres further north (Antiparos and Patmos), which were active during this time interval (Vougioukalakis et al., 2019). Biostratigraphy shows that the youngest layer with dateable fossils (bio-event, the last common occurrence of Sphenolithus spp., Van Hinsbergen et al., 2004) in the Neogene sedimentary rocks is 3.54 Ma old (GTS2012, Gradstein et al., 2012). The diatomite Unit II from Calvo et al. (2012) on top of the oldest volcanoclastic deposit from the north-eastern coast of Milos is constrained within 2.83-3.19 Ma. These data suggest that the oldest products must be older than 2.83 Ma and younger than 3.54 Ma. Our oldest $^{40}Ar/^{39}Ar$ ages of this study displayed a wide range of 3.41-4.10 Ma that, are probably not correct due to the alteration of the samples. Alteration might induce Ar loss and that would imply that the age is even older than 3.4-4.1 Ma. The age of 3.50 ± 0.14 Ma given by Fytikas et al. (1986) for an andesite pillow lava or dyke has been discussed above and probably belongs to a series of basaltic andesite intrusions in the younger dacitic-rhyolitic deposits of Profitis Illias (~ 3.08 Ma, Fytikas et al., 1986), and therefore the 3.5 Ma age is probably not correct (e.g. Stewart, 2003). Fytikas et al. (1986) measured one sample from Kimolos (Figure 2 and 3) with an age of 3.34 Ma. Furthermore, Ferrara et al. (1980) reported an age of 3.15 Ma for a lithic clast derived from the Petalia intrusion in the Kastro volcaniclastics of Polyegos. If we assume that this reported age is a cooling age, volcanism in the Milos VF must have started before 3.15 Ma. Although age constraints for phase 1 both from the Neogene sedimentary rocks and the dated volcanic samples are poor, the evidence at this stage would suggest that phase 1, and hence volcanism in the Milos VF started around ~3.34 Ma ago.

Phase 1 (~3.34-3.06 Ma) is similar to the basal pyroclastic series of Fytikas et al., 1986, and the submarine felsic cryptodome/pumice cone facies of Stewart and McPhie (2006). We note that two submarine felsic cryptodome/pumice cone volcanoes (Dhemenghaki and Bombara) were active during phase 5 (see below). This point was also noted by Stewart and McPhie, who stated that the cycles of Fytikas et al. (1986) were actually interfingering with other "cycles". The Phase 1

https://doi.org/10.5194/gchron-2020-30
Preprint. Discussion started: 13 October 2020

deposits are deposited conformably and unconformably on the Neogene sedimentary rocks (Van Hinsbergen et al., 2004). East of the Fyriplaka Fault (Figure 2), the phase 1 deposits overlie unconformably the Mesozoic metamorphic basement (Stewart, 2003). The stratigraphic columns (after Stewart and McPhie, 2006, Fig. 14B) show that a mixture of felsic pumice and sandstone (~100 m thick) was deposited between the Profitis Illias dacite (3.06 ± 0.02 Ma) and the Kleftiko andesitic or basaltic andesitic dyke (2.66 ± 0.01 Ma), suggesting at least one pulse of volcanic activity between 2.66 and 3.06 Ma or erosion products from the previous eruptions. Submarine eruptions occurred during this phase from broadly circular submarine pumice cones with dacitic to rhyolitic magma compositions (Stewart and McPhie, 2006). The products are thick intervals of felsic pumice breccia that were either formed by gravity currents or deposition of pumices from suspension. These pumice breccias were later intruded by dacitic to rhyolitic cryptodomes and sills (Stewart and McPie, 2006). The main eruption centre of this phase is the Profitis Illias volcano (Fig. 2), The amount of volcanic material that phase 1 contributed to the Milos VF is difficult to establish, since the volcanic rocks are strongly weathered (e.g. Fytikas et al., 1986; Stewart and McPhie, 2006).

Phase 2 (2.66-2.50 Ma) was considered as a phase because of a long volcanic quiescence period (Q1) of 0.3 Ma after phase 1. The Fylakopi pumice cone volcano and Kalogeros cryptodome of phase 2 in the north-eastern part of Milos, were probably simultaneously active from 2.66 to 2.62 Ma. These pumice cone/cryptodome volcanoes are comparable to the Profitis Ilias volcano of phase 1 (Figure 14B). All of the deposits of phase 1 and 2 were submarine, most of them below wave base (up to several hundred meters water depth), although maybe some volcanic structures were large enough to become subaerial that were subsequently quickly eroded (Stewart and McPhie, 2006). These two phases could contribute 3-12 km^3 DRE to the Milos VF (Fig. 12).

Phase 3 (2.50-2.36 Ma) forms together with phase 4 the "complex of domes and lava flows" defined by Fytikas et al. (1986) (Fig. 4 and 15). This phase includes the Mavros Kavos and Mavro Vouni domes in the south-western part of Milos. These domes form high-aspect ratio deposits with a roughly concentric structure of a coherent core, 30-40 m thick layer which is flow banded and a monomeric breccia (Stewart and McPhie, 2006). The deposits of these domes intrude and overlie the phase 1 and 2 deposits. The composition of the deposits is andesitic-dacitic (this study and Stewart and McPhie, 2006). These deposits are interpreted as submarine domes, which were extruded onto the sea floor or into shallow unconsolidated pumice rich sediments. The volume estimate of these deposits was only approximately 1-2 km^3 DRE.

Phase 4 (2.13-1.90 Ma) started after a volcanic quiescence period of ~200 kyrs (Q2) since phase 3. Phase 4 has similar submarine dome extrusions as phase 3, but the volcanism of phase 4 moved to the north-western (Triades lava dome) and north-eastern (Adamas lava dome) parts of the Milos VF. Approximately 4-13 km^3 DRE was added to the Milos VF during this phase.

Phase 5 (1.90-1.60 Ma) consists of two rhyolitic pumice cone/cryptodome structures (Dhemenghaki and Bombarda) in the north-eastern part of Milos and are similar to the phase 1-2 volcanism. For the Bombarda centre a large age range is reported in the literature (1.71-2.15 Ma, Fig. 14B). We were not successful to date samples from the Bombarda centre, but Rinaldi and Campos Venuti (2003) reported that an age of 1.71 Ma is the best approximation based on other stratigraphic information. For the Dhemenghaki centre we reported a $^{40}Ar/^{39}Ar$ age of 1.825 ± 0.002 Ma from an obsidian. These centres all developed in a submarine setting, as the intercalated sediments from the northern coast of Milos show (Diatomite layer III in Fig. 2 and 3 of Calvo et al., 2012). This phase contains the same volcano type as the phase 1 and 2, but is constructed from rhyolitic material only. This phase resulted in an addition of approximately 5-18 km^3 DRE to the Milos VF.

Phase 6 (1.60-1.48 Ma) consists of two submarine-to-subaerial lava dome extrusions (Kantaro and Korakia in the northwest and northeast of Milos, respectively) that are dacitic and andesitic in composition. The petrological observations of the dacite sample G15M0019 and -20 of the Kantaro dome show the presences of the olivine-clinopyroxene-orthopyroxene cumulates and the amphibole-biotite reaction rims (supplementary material I). The andesite of Korakia dome (G15M0029) has a groundmass of acicular plagioclase and plagioclase phenocrysts with sieve textures. In addition, the intermediate composition of phase 6 is similar to that of phase 1-3. These petrological and geochemical characters of phase 6 indicate the magma mixing

https://doi.org/10.5194/gchron-2020-30
Preprint. Discussion started: 13 October 2020

in these andesitic-dacitic units, that a mafic magma from the deep crust likely injected into the shallow chamber beneath the Kantato and Korakia domes.

During phase 6, volcanism on Milos began to change to subaerial by the formation of these domes (e.g. Stewart and McPhie, 2006). These domes structures have the characteristics of subaerial domes with an extent of 2.5-10 km^2 and are maximal 250-350 m thick in the proximal part (Stewart and McPhie, 2006). Single domes have a massive core and flow banded rind surrounded by an in situ autobreccia zone. Phase 6 volcanic units only added a small volume of 0.5-2.5 km^3 DRE to the Milos VF (Figure 12). This phase is followed by a period of no volcanic activity of approximately 400 kyrs (Q3 in Figure 15).

Phase 7 (1.04-0.97 Ma) contains two eruption centres. The older one produced the subaerial rhyolitic lavas of Halepa (1.04 ± 0.01 Ma) in the south of Milos, which has similar geochemical characteristics to that of phase 5. The second eruption centre is the dacitic Plakes dome in the north of Milos (0.97 ± 0.06 Ma, Fytikas et al., 1986), of which the geochemical character is comparable to that of phase 6. We include them into one phase since their eruptive ages are so closed, even though the geochemical characteristics of both domes are different. Fytikas et al. (1986) included these in the PSLD (Figure 14A and 15). The Plakes volcano is probably the last volcano erupting in a submarine environment on Milos, whereas the rhyolitic lavas of Halepa are subaerial (Stewart and McPhie, 2006). Also, this phase is small in volume (1-3 km^3, Figure 12) and is followed by the fourth period of quiescence (Q4 in Figure 15) of approximately 300 kyrs.

Phase 8 (0.63-0.32 Ma) consists of two subaerial eruption centres with biotite bearing rhyolites. The first one, described by Campos Venuti and Rossi (1996) is the Kalamos lava dome (0.412 ± 0.004 Ma) that underlies the Fyriplaka complex deposits at Fyriplaka beach (phase 9, see below). The Trachilas complex in the northern part of Milos was active for approximately 300 kyrs (0.63-0.32 Ma). The evolution of this complex starts with phreatic eruptions which became less explosive over time (Fytikas et al., 1986). In the last phase rhyolitic lavas filled up the crater area and did breach the northern tuff cone walls. This phase only added a small volume (1-2 km^3 DRE) of material to the Milos VF. Between phase 8 and 9 there is another quiescence period (Q5) of ~200kyrs (Fig. 15).

The youngest phase, 9 (0.11 Ma-present), is characterized by subaerial eruptions of biotite phyric rhyolite from the Fyriplaka complex and was studied in detail by Campos Venuti and Rossi (1996). This complex is constructed on a paleosol that developed in a phreatic deposit ("Green Lahar", Fytikas et al., 1986) or lies directly on the metamorphic basement. Campos Venuti and Rossi (1996) indicated that the stratigraphic order is: Fyriplaka and Gheraki tuff rings, Fyriplaka lava flow, composed tuff cone of Tsigrado-Provatas. The tuff ring of Fyriplaka was divided into 3 members, with on top the deposits of the Tsigrado tuff cone. The total estimated volume of volcanic material is 0.18 km^3 DRE. The boundary between the Fyriplaka and Tsigrado tuff cones is characterized by a marked erosive unconformity. The composition of the volcanic products of this phase is very constant (Fig. 10-11), this was also noted by Fytikas et al (1986) and Campos Venuti and Rossi (1996). The products from Fyriplaka and Tsigrado cones are covered with a paleosol rich in archeological remains and a phreatic deposit consisting largely of greenschist metamorphic fragments. According to Campos Venuti and Rossi (1996), the Fyriplaka cone was quickly build by phreatic and phreatomagmatic eruptions, as there are no paleosols observed between the different units. However, our data do suggest a large range in ages between 0.11 and 0.06 Ma. Fytikas et al. (1986) also reported a range between 0.14 and 0.09 Ma. These ages are inconsistent with the "Green Lahar" age of 27 kyrs (Principe et al., 2002), suggesting that the "Green Lahar" deposit consists of many different phreatic eruption layers that were formed over a period of more than 0.4 Ma, as the Kalamos lava of phase 8 is underlain by a green phreatic eruption breccia (Campos Venuti and Rossi 1996). We therefore conclude that between phase 8 and 9 phreatic eruptions occurred, predominately in the eastern part of Milos until historical times (200 BC – 200 AD, Traineau and Dalabakis, 1989).

4.4 Temporal variations in the major element composition of the volcanic units of the Milos VF

Alteration of the submarine deposits is widespread on Milos, and although we tried to sample material as fresh as possible, there are still indications that some of our samples are not pristine. This is clearly demonstrated in the SiO_2 versus K_2O and

https://doi.org/10.5194/gchron-2020-30
Preprint. Discussion started: 13 October 2020

BaO diagrams (Fig. 16A and –B). Two samples G15M0022 and -21 of the Triades lave dome of phase 4, have anomalously high BaO (~0.35 wt. %) and K_2O (6-7 wt.%) contents, despite these samples have a relatively low LOI. (<0.2 wt.%). We will not discuss these samples below. Some volcanic units (Profitis Illias, Mavro Vouni and Bombarda) are not shown in Figures 16 as we were unable to obtain fresh samples and published data are lacking. The major element compositions of the volcanic units of Filakopi and Plakes can be obtained from Stewart and McPhie (2003) and Fytikas et al. (1986), respectively, and are shown in Figure 16 together with our data.

The pumice cone/cryptodome volcanic units of phase 1-3 and the dome lavas of phase 4-7 are similar in composition. The SiO_2 content of the cyptodome units of phase 1-3 shows a narrow range of 64-70 wt.%, excluding the basaltic andesitic sample G15M0016 (SiO_2: 55.72 wt.%) of the dyke near Kleftiko. The CaO content of the cryptodome units decreased from 5.9 to 2.9 wt.% from Phase 1 to 3, whereas the Na_2O content increased from 3.3 to 4.2 wt.%. In addition, the petrographic observations of these rocks suggest a pyroxene-amphibole sequence of crystallization from phase 1 to 3 (supplementary material I). In combination with the intermediate composition, the fractionation process of phase 1-3 in these cryptodome and dome units could be fed by a magma system in the relatively deep crust. This hypothesis is in agreement with the modelling results of Fytikas et al. (1986) for the Pliocene volcanic cycles of the Milos VF. However, the limited compositional data of the pumiceous units of the Profitis Illias (~3.08 Ma) and Mavro Vouni (2.50 Ma) volcanoes inhibit us to fully discuss the geochemical characters of the first three phases of the Milos VF.

The volcanic units of phase 8 and 9 both are rhyolitic (SiO_2 wt.%>72) in composition, but their geochemical characteristics are different. There are subtle differences between TiO_2/Fe_2O_3 and CaO/Al_2O_3 ratios, suggesting that the fractionation or resorption of biotite and the presence of oxide minerals could explain these subtle differences.

Although rhyolites have erupted throughout the whole history of the Milos VF, the volumes were most pronounced during phase 1. However, during phase 2-9 there is a clear shift to smaller volumes of magma and the tendency to become more felsic over time (Fig. 12).

4.5 Temporal variations in the volumetric volcanic output rate of the Milos VF.

The volume estimates of the Milos VF are hampered by limited exposure of several volcanic units and unknown age relationships. Therefore, not all units can be attributed to a certain volcano. Furthermore, we also do not know how much volcanic material was lost through transport by air, sea currents and erosion. Given the large errors on these estimates, we only considered the rough difference in density between extruded magma and the calculated DRE values. The volumetric contributions of the islands Polygos, Kimolos and Antimilos are not considered here. Therefore, the discussion here only provides a first order estimate of the onshore extruded magma volume. Taken into account all these limitations, our age data and the volume estimates by Stewart and McPhie (2006) likely indicate at least three periods of different long term volumetric volcanic output rates (Q_e): 0.5-1.8$\times10^{-5}$ km^3/yr of Phase 1-3 (~3.34- 2.36 Ma), 2.0-6.6$\times10^{-5}$ km^3/yr of Phase 4-5 (2.13-1.60 Ma) and 0.2-0.4$\times10^{-5}$ km^3/yr of Phase 6-9 (1.60 Ma-present) (Fig. 12). This suggests that the Milos VF has a low long-term Q_e of 0.2-6.6$\times10^{-5}$ km^3/yr. This is at least 2-3 orders lower than the average for rhyolitic systems (4.0$\times10^{-3}$ km^3/yr) and the mean for continental arcs (~70$\times10^{-3}$ km^3/yr) with a range of 8$\times10^{-6}$ – 9$\times10^{-2}$ km^3/yr (White et al., 2006). Milos overlaps with the lowest Q_e values of the study of White et al. (2006). There are large variations in Q_e in the Milos VF: during phase 5 (1.90-1.60 Ma) the Q_e is relatively high, whereas the last 1.6 Myrs (phase 6-9) the volumetric volcanic output rate is more than an order of magnitude lower.

No data are available for the ratio between intruded magma in the crust below Milos and extruded volcanics (I:E). White et al. (2006) argue that a ratio of 5:1 is probably a realistic estimate for most volcanic centres and that this ratio can be higher in volcanic centres constructed on continental crust. This would result in a magma supply rate from the mantle beneath the Milos VF in the order of 0.1-3.3$\times10^{-4}$ km^3/yr. Compared with other SAVA volcanic centres, Druitt et al. (2019) reported a long-term average magma supply rate of approximately 1$\times10^{-3}$ km^3/yr beneath the Kameni islands of the caldera of Santorini.

https://doi.org/10.5194/gchron-2020-30
Preprint. Discussion started: 13 October 2020

Considering our estimate of the volcanic volume on the Milos VF is the minimum value, this rate is comparable to that of the Milos. Besides the case of Santorini VF, no other information on the long-term average magma supply rate of other volcanic centres of the SAVA is available to our knowledge.

Given that the island of Milos is approximately 15 km long (W-E), this results in a magma production rate over the last ~3.34 Ma of approximately 0.7-22 $km^3.km^{-1}.Myr^{-1}$. Although this magma production rate per km arc length is the onshore estimate for the Milos VF, it is still significant lower than for oceanic arcs: 157-220 $km^3.Myr^{-1}.km^{-1}$ (Jicha and Jagoutz, 2015). For continental arcs the long-term magma production rate is more difficult to establish because magmatism is cyclic, and short periods (5-20 Ma) of intense magmatism ("flare ups") with 85 $km^3.km^{-1}.Myr^{-1}$are alternating with periods of 25-50 Ma of low magma production rate of 20 $km^3.km^{-1}.Myr^{-1}$ (e.g. Jicha and Jagoutz, 2015). The periods of low magma production overlap with the magma production rates beneath the Milos VF over the past ~3.34 Ma.

5 Conclusion

This study reports twenty-one new $^{40}Ar/^{39}Ar$ ages and major element data for 10 volcanic units of the Milos Volcanic Field. In combination with published age data and volcanic facies descriptions, this allows us to divide the volcanic evolution of the Milos VF into 9 phases and 5 quiescence periods. Here we define a phase as a period that contains 1-2 volcano types (e.g. pumice cone/crypto dome, lava dome, tuff cone) in a certain area of the Milos VF (NW, NE, SE or SW part) and a quiescence period when there is no or limited volcanic activity for more than 200 kyrs.

Phase 1 (~3.34-3.06 Ma) and Phase 2 (2.66-2.50 Ma) contain the same volcano type, submarine pumice cone/cryptodome, but the volcanic units of phase 1 and 2 are located in the south-western and north-eastern parts of the Milos VF, respectively. There is a long quiescence period of ~400 kyrs between phase 1 and 2.

Phase 3 (2.50-2.36 Ma) resulted in the construction of submarine andesitic-dacitic domes in the south-western part of the Milos VF. The lavas of phase 3 are extruded onto the seafloor or intruded in soft pumice rich sediments of phase 1. After phase 3, a period of ~200 kyrs of volcanic quiescence followed.

Phase 4 (2.13-1.90 Ma), Phase 5 (1.90-1.60 Ma) and Phase 6 (1.60–1.48 Ma) volcanism took place in the north-eastern and north-western parts of the Milos VF. Phase 4 and 6 consist of andesitic to dacitic domes, whereas Phase 5 is comprised of rhyolitic pumice cone/cryptodome volcanoes. Phase 6 contains the oldest subaerial dacitic dome (Kantaro dome). After phase 6, there is a ~400 kyrs interval of no or limited volcanic eruptions.

Phase 7 (1.04-0.97 Ma) consists of two subaerial volcanic units: the rhyolitic Halepa and the dacitic Plakes lava domes in the southern and northern parts of the Milos VF, respectively. Between phase 7 and 8 is a period of volcanic quiescence of ~350 kyrs.

Phase 8 (0.63-0.32 Ma) covers the formation period of the subaerial rhyolitic Trachilas complex in the north-eastern part of the Milos VF and the rhyolitic Kalamos lava in the southeast. A ~200kyrs period of volcanic quiescence occurred between phase 8 and 9.

Phase 9 (0.11 Ma-present) consists of subaerial rhyolitic lava and pyroclastic deposits of the Fyriplaka complex in the south-eastern part of the Milos VF. During phase 8 and 9 there could be a few phreatic eruptions, mainly in the south-eastern part of Milos. The different volcanic locations and geochemical characters between phase 8 and 9 suggest the different magma sources for these two phases.

During the evolution of the Milos VF volcanic rocks changed over time in composition from more mafic basaltic-andesite-rhyolite volcanism to mainly rhyolite. The volcanic complex of Milos was largely (~85% by volume) constructed during ~3.34-1.6 Ma. From 1.6 Ma to present, only small volumes of rhyolitic magma were added from different eruption vents. The long term volumetric volcanic output rate (Q_e) of Milos is 0.2-6.6$\times 10^{-5}$ km^3/yr, 2-3 orders of magnitude lower than the average for rhyolitic systems and continental arcs.

https://doi.org/10.5194/gchron-2020-30
Preprint. Discussion started: 13 October 2020

Acknowledgement

We would like to thank Roel van Elsas with the assistance of rock crushing and mineral separation. Kiki Dings helped with the XRF bead preparation and measurements. Lara Borst and Onno Postma assisted with the $^{40}Ar/^{39}Ar$ dating. We acknowledge the Greek Institute of Geology and Mineral Exploration (IGME) for permission to conduct fieldwork on Milos. Xiaolong Zhou would like to acknowledge a grant no. 201506400055 from the China Scholarship Council (CSC). The $^{40}Ar/^{39}Ar$ facility of the VU is covered by NWO grant 834.09.004. This research benefitted from funding from the European Research Council under the European Union's Seventh Framework Programme (FP7/2007-2013)/ERC grant agreement n° 319209.

https://doi.org/10.5194/gchron-2020-30
Preprint. Discussion started: 13 October 2020

706 **References**

707 Alfieris, D., Voudouris, P., and Spry, P.G.: Shallow submarine epithermal Pb-Zn-Cu-Au-Ag-Te mineralization on western
708 Milos Island, Aegean Volcanic Arc, Greece: Mineralogical, geological and geochemical constraints: Ore Geology
709 Reviews, v. 53, p. 159–180, doi:10.1016/j.oregeorev.2013.01.007, 2013.
710 Angelier, J., Cantagrel, J.-M., and Vilminot, J.-C.: Neotectonique cassante et volcanisme plio-quaternaire dans l'arc egeen
711 interne; l'ile de Milos (Grece): Bulletin de la Société Géologique de France, v. 7, p. 119–124, 1977.
712 Arias, A., Oddone, M., Bigazzi, G., Di Muro, A., Principe, C., and Norelli, P.: New data for the characterization of Milos
713 obsidians: Journal of Radioanalytical and Nuclear Chemistry, v. 268, p. 371–386, doi:10.1007/s10967-006-0183-9,
714 2006.
715 Bas, M.J.L., Maitre, R.W.L., Streckeisen, A., and Zanettin, B.: A chemical classification of volcanic rocks based on the total
716 alkali-silica diagram: Journal of Petrology, v. 27, p. 745–750, doi:10.1093/petrology/27.3.745, 1986.
717 Bigazzi, G., and Radi, G.: Datazione con le tracce di fissione per l'identificazione della provenienza dei manufatti di
718 ossidiana: Rivista di Scienze Preistoriche, v. 36/1–2, p. 223–250, 1981.
719 Calvo, J.P., Triantaphyllou, M. V., Regueiro, M., and Stamatakis, M.G.: Alternating diatomaceous and volcaniclastic
720 deposits in Milos Island, Greece. A contribution to the upper Pliocene-lower Pleistocene stratigraphy of the Aegean
721 Sea: Palaeogeography, Palaeoclimatology, Palaeoecology, v. 321–322, p. 24–40, doi:10.1016/j.palaeo.2012.01.013,
722 2012.
723 Campos Venuti, M., and Rossi, P.L.: Depositional facies in the Fyriplaka rhyolitic tuff ring, Milos Island (Cyclades,
724 Greece): Acta Vulcanologica, v. 8, p. 173–192, 1996.
725 Cassata, W.S., and Renne, P.R.: Systematic variations of argon diffusion in feldspars and implications for
726 thermochronometry: Geochimica et Cosmochimica Acta, v. 112, p. 251–287, doi:10.1016/j.gca.2013.02.030, 2013.
727 Cole, P.D., Calder, E.S., Sparks, R.S.J., Clarke, A.B., Druitt, T.H., Young, S.R., Herd, R.A., Harford, C.L., and Norton,
728 G.E.: Deposits from dome-collapse and fountain-collapse pyroclastic flows at Soufrière Hills Volcano, Montserrat:
729 Geological Society, London, Memoirs, v. 21, p. 231–262, 2002.
730 Crosweller, H.S., Arora, B., Brown, S.K., Cottrell, E., Deligne, N.I., Guerrero, N.O., Hobbs, L., Kiyosugi, K., Loughlin,
731 S.C., and Lowndes, J.: Global database on large magnitude explosive volcanic eruptions (LaMEVE): Journal of
732 Applied Volcanology, v. 1, p. 4, 2012.
733 Doglioni, C., Agostini, S., Crespi, M., Innocenti, F., Manetti, P., Riguzzi, F., and Savaşçın, M.Y.: On the extension in
734 western Anatolia and the Aegean sea On the extension in western Anatolia and the Aegean sea: Journal of Virtual
735 Explorer, v. 07, p. 167–181, doi:10.3809/jvirtex.2002.00049, 2002.
736 Druitt, T.H., Edwards, L., Mellors, R.M., Pyle, D.M., Sparks, R.S.J., Lanphere, M., Davies, M., and Barreirio, B.: Santorini
737 Volcano: Geological Society Memoir, v. 19, http://pubs.er.usgs.gov/publication/70094778, 1999.
738 Druitt, T.H., Pyle, D.M., and Mather, T.A.: Santorini Volcano and its Plumbing System: Elements, v. 15, p. 177–184,
739 doi:10.2138/gselements.15.3.177, 2019.
740 Duermeijer, C.E., Nyst, M., Meijer, P.T., Langereis, C.G., and Spakman, W.: Neogene evolution of the Aegean arc:
741 Paleomagnetic and geodetic evidence for a rapid and young rotation phase: Earth and Planetary Science Letters, v.
742 176, p. 509–525, doi:10.1016/S0012-821X(00)00023-6, 2000.
743 Ferrara, G., Fytikas, M., Giuliani, O., and Marinelli, G.: Age of the formation of the Aegean active volcanic arc: Thera and
744 the Aegean world II, v. 2, p. 37–41, 1980.
745 Flowers, R.M., Bowring, S.A., Tulloch, A.J., and Klepeis, K.A.: Tempo of burial and exhumation within the deep roots of a
746 magmatic arc, Fiordland, New Zealand: Geology, v. 33, p. 17–20, doi:10.1130/G21010.1, 2005.
747 Francalanci, L., Vougioukalakis, G.E., Fytikas, M., Beccaluva, L., Bianchini, G., and Wilson, M.: Petrology and
748 volcanology of Kimolos and Polyegos volcanoes within the context of the South Aegean arc, Greece: SPECIAL

https://doi.org/10.5194/gchron-2020-30
Preprint. Discussion started: 13 October 2020

PAPERS-GEOLOGICAL SOCIETY OF AMERICA, v. 418, p. 33, 2007.

Francalanci, L., and Zellmer, G.F.: Magma Genesis at the South Aegean Volcanic Arc: Elements, v. 15, p. 165–170, doi:10.2138/gselements.15.3.165, 2019.

Frey, H.M., Lange, R.A., Hall, C.M., and Delgado-Granados, H.: Magma eruption rates constrained by 40Ar/39Ar chronology and GIS for the Ceboruco-San Pedro volcanic field, western Mexico: Bulletin of the Geological Society of America, v. 116, p. 259–276, doi:10.1130/B25321.1, 2004.

Fytikas, M., Giuliani, O., Innocenti, F., Marinelli, G., and Mazzuoli, R.: Geochronological data on recent magmatism of the Aegean Sea: Tectonophysics, v. 31, p. T29–T34, doi:10.1016/0040-1951(76)90161-X, 1976.

Fytikas, M., Innocenti, F., Kolios, N., Manetti, P., Mazzuoli, R., Poli, G., Rita, F., and Villari, L.: Volcanology and petrology of volcanic products from the island of Milos and neighbouring islets: Journal of Volcanology and Geothermal Research, v. 28, p. 297–317, doi:10.1016/0377-0273(86)90028-4, 1986.

Fytikas, M.: Updating of the geological and geothermal research on Milos island: Geothermics, v. 18, p. 485–496, doi:10.1016/0375-6505(89)90051-5, 1989.

Gradstein, F.M., Ogg, J.G., Schmitz, M., and Ogg, G.: The Geologic time scale, 2012: elsevier, v. 50, 50-4449-50–4449 p., doi:10.5860/choice.50-4449, 2013.

Grasemann, B., Huet, B., Schneider, D.A., Rice, A.H.N., Lemonnier, N., and Tschegg, C.: Miocene postorogenic extension of the Eocene synorogenic imbricated Hellenic subduction channel: New constraints from Milos (Cyclades, Greece): Bulletin of the Geological Society of America, v. 130, p. 238–262, doi:10.1130/B31731.1, 2018.

Grove, M., and Harrison, T.M.: ^{40}Ar* diffusion in Fe-rich biotite: American Mineralogist, v. 81, p. 940–951, 1996.

Hayes, G.P., Moore, G.L., Portner, D.E., Hearne, M., Flamme, H., Furtney, M., and Smoczyk, G.M.: Slab2, a comprehensive subduction zone geometry model: Science, v. 362, p. 58–61, doi:10.1126/science.aat4723, 2018.

Hildreth, W., and Lanphere, M.A.: Potassium-argon geochronology of a basalt-andesite-dacite arc system: The Mount Adams volcanic field, Cascade Range of southern Washington: Geological Society of America Bulletin, v. 106, p. 1413–1429, 1994.

Hildreth, W., Fierstein, J., and Lanphere, M.: Eruptive history and geochronology of the Mount Baker volcanic field, Washington: Geological Society of America Bulletin, v. 115, p. 729–764, 2003a.

Hildreth, W., Lanphere, M.A., and Fierstein, J.: Geochronology and eruptive history of the Katmai volcanic cluster, Alaska Peninsula: Earth and Planetary Science Letters, v. 214, p. 93–114, doi:10.1016/S0012-821X(03)00321-2, 2003b.

Hora, J.M., Singer, B.S., Jicha, B.R., Beard, B.L., Johnson, C.M., de Silva, S., and Salisbury, M.: Volcanic biotite-sanidine 40Ar/39Ar age discordances reflect Ar partitioning and pre-eruption closure in biotite: Geology, v. 38, p. 923–926, doi:10.1130/G31064.1, 2010.

IJlst, L.: A laboratory overflow-centrifuge for heavy liquid mineral separation: American Mineralogist, v. 58, p. 1088–1093, 1973.

Irvine, T.N.J., and Baragar, W.R.A.: A guide to the chemical classification of the common volcanic rocks: Canadian journal of earth sciences, v. 8, p. 523–548, 1971.

Jicha, B.R., and Jagoutz, O.: Magma production rates for intraoceanic arcs: Elements, v. 11, p. 105–112, doi:10.2113/gselements.11.2.105, 2015.

Kilias, S.P., Naden, J., Cheliotis, I., Shepherd, T.J., Constandinidou, H., Crossing, J., and Simos, I.: Epithermal gold mineralisation in the active Aegen volcanic arc: The Profitis Ilias deposits, Milos Island, Greece: Mineralium Deposita, v. 36, p. 32–44, doi:10.1007/s001260050284, 2001.

Koppers, A.A.P.: ArArCALC-software for ^{40}Ar/^{39}Ar age calculations: Computers and Geosciences, v. 28, p. 605–619, doi:10.1016/S0098-3004(01)00095-4, 2002.

Kornprobst, J., Kienast, J.-R., and Vilminot, J.-C.: The high-pressure assemblages at Milos, Greece: Contributions to

https://doi.org/10.5194/gchron-2020-30
Preprint. Discussion started: 13 October 2020

Mineralogy and Petrology, v. 69, p. 49–63, doi:10.1007/bf00375193, 1979.

Kuiper, K.F., Deino, A., Hilgen, F.J., Krijgsman, W., Renne, P.R., and Wijbrans, J.R.: Synchronizing Rock Clocks of Earth History: Science, v. 320, p. 500–504, doi:10.1126/science.1154339, 2008.

Lee, J.Y., Marti, K., Severinghaus, J.P., Kawamura, K., Yoo, H.S., Lee, J.B., and Kim, J.S.: A redetermination of the isotopic abundances of atmospheric Ar: Geochimica et Cosmochimica Acta, v. 70, p. 4507–4512, doi:10.1016/j.gca.2006.06.1563, 2006.

Lee, J.K.W.: Ar–Ar and K–Ar Dating BT - Encyclopedia of Scientific Dating Methods, *in* Jack Rink, W. and Thompson, J.W. eds., Dordrecht, Springer Netherlands, p. 58–73, doi:10.1007/978-94-007-6304-3_40, 2015.

Mark, D.F., Barfod, D., Stuart, F.M., and Imlach, J.: The ARGUS multicollector noble gas mass spectrometer: Performance for 40Ar/39Ar geochronology: Geochemistry, Geophysics, Geosystems, v. 10, p. 1–9, doi:10.1029/2009GC002643, 2009.

Matsuda, J., Senoh, K., Maruoka, T., Sato, H., and Mitropoulos, P.: K-Ar ages of the Aegean the volcanic rocks and arc-trench system their implication for the arc-trench system: Geochemical Journal, v. 33, p. 369–377, 1999.

McKenzie, D.: Active tectonics of the Alpine—Himalayan belt: the Aegean Sea and surrounding regions: Geophysical Journal International, v. 55, p. 217–254, 1978.

Meulenkamp, J.E., Wortel, M.J.R., van Wamel, W.A., Spakman, W., and Hoogerduyn Strating, E.: On the Hellenic subduction zone and the geodynamic evolution of Crete since the late Middle Miocene: Tectonophysics, v. 146, p. 203–215, doi:10.1016/0040-1951(88)90091-1, 1988.

Min, K., Mundil, R., Renne, P.R., and Ludwig, K.R.: A test for systematic errors in $^{40}Ar/^{39}Ar$ geochronology: Geochimica et Cosmochimica Acta, v. 64, p. 73–98, 2000.

Nicholls, I.A.: Santorini volcano, greece - tectonic and petrochemical relationships with volcanics of the Aegean region: Tectonophysics, v. 11, p. 377–385, doi:10.1016/0040-1951(71)90026-6, 1971.

Peccerillo, A., and Taylor, S.R.: Geochemistry of eocene calc-alkaline volcanic rocks from the Kastamonu area, Northern Turkey: Contributions to Mineralogy and Petrology, v. 58, p. 63–81, doi:10.1007/BF00384745, 1976.

Pe-Piper, G., and Piper, D.J.W.: Neogene backarc volcanism of the Aegean: New insights into the relationship between magmatism and tectonics: Geological Society of America Special Papers, v. 418, p. 17–31, doi:10.1130/2007.2418(02) , 2007.

Pe-Piper, G., and Piper, D.J.W.: The effect of changing regional tectonics on an arc volcano: Methana, Greece: Journal of Volcanology and Geothermal Research, v. 260, p. 146–163, doi:10.1016/j.jvolgeores.2013.05.011, 2013.

Principe C, Arias A, Zoppi U.: Origin, transport and deposition of a debris avalanche de- posit of phreatic origin on Milos Island (Greece). Montagne Pelee 1902-2002, Explosive Vol- canism in Subduction Zones, Martinigue 12-16 May, 2002. Abstracts p. 71, 2002.

Rinaldi, M., and Venuti, M.C.: The submarine eruption of the Bombarda volcano, Milos Island, Cyclades, Greece: Bulletin of Volcanology, v. 65, p. 282–293, doi:10.1007/s00445-002-0260-z, 2003.

Rivera, T.A., Storey, M., Zeeden, C., Hilgen, F.J., and Kuiper, K.: A refined astronomically calibrated 40Ar/39Ar age for Fish Canyon sanidine: Earth and Planetary Science Letters, v. 311, p. 420–426, doi:10.1016/j.epsl.2011.09.017, 2011.

Rontogianni, S., Konstantinou, N.S., Melis, C.P., and Evangelidis.: Slab stress field in the Hellenic subduction zone as inferred from intermediate-depth earthquakes: Earth, Planets and Space, v. 63, p. 139–144, doi:10.5047/eps.2010.11.011, 2011.

Schaen, A., Jicha, K., Hodges et al.: Interpreting and reporting 40Ar/39Ar geochronologic data: GSA Bulletin, doi:10.1130/B35560.1, 2020.

Singer, B.S., Thompson, R.A., Dungan, M.A., Feeley, T.C., Nelson, S.T., Pickens, J.C., Brown, L.L., Wulff, A.W., Davidson, J.P., and Metzger, J.: Volcanism and erosion during the past 930 k.y. at the Tatara–San Pedro complex,

https://doi.org/10.5194/gchron-2020-30
Preprint. Discussion started: 13 October 2020

Chilean Andes: Geological Society of America Bulletin, v. 109, p. 127–142, doi:10.1130/0016-7606(1997)109<0127:VAEDTP>2.3.CO;2, 1997.

Sonder, R.A.: Zur Geologie and Petrographie der Inselgruppe yon Milos: Zeitschr. Volc., v. 8, p. 11–231, 1924.

Spakman, W., Wortel, M.J.R., and Vlaar, N.J.: The Hellenic Subduction Zone: A tomographic image and its geodynamic implications: Geophysical Research Letters, v. 15, p. 60–63, doi:10.1029/GL015i001p00060, 1988.

Stewart, A.L., and McPhie, J.: Internal structure and emplacement of an Upper Pliocene dacite cryptodome, Milos Island, Greece: Journal of Volcanology and Geothermal Research, v. 124, p. 129–148, doi:10.1016/S0377-0273(03)00074-X, 2003.

Stewart, A.L.: Volcanic Facies Architecture and Evolution of Milos, Greece: Ph.D. thesis, University of Tasmania, 1–240 p, 2003.

Stewart, A.L., and McPhie, J.: Facies architecture and Late Pliocene – Pleistocene evolution of a felsic volcanic island, Milos, Greece: Bulletin of Volcanology, v. 68, p. 703–726, doi:10.1007/s00445-005-0045-2, 2006.

Traineau, H., and Dalabakis, P.: Mise en evidence d'une eruption phreatique historique sur l'ile de Milos (Grece): CR Acad Sci Paris, p. 1–38, 1989.

Van Hinsbergen, D.J.J., Snel, E., Garstman, S.A., Marunţeanu, M., Langereis, C.G., Wortel, M.J.R., and Meulenkamp, J.E.: Vertical motions in the Aegean volcanic arc: Evidence for rapid subsidence preceding volcanic activity on Milos and Aegina: Marine Geology, v. 209, p. 329–345, doi:10.1016/j.margeo.2004.06.006, 2004.

Vougioukalakis, G.E., Satow, C.G., and Druitt, T.H.: Volcanism of the South Aegean volcanic arc: Elements, v. 15, p. 159–164, 2019.

Wendt, I., and Carl, C.: The statistical distribution of the mean squared weighted deviation: Chemical Geology: Isotope Geoscience Section, v. 86, p. 275–285, doi:10.1016/0168-9622(91)90010-T, 1991.

White, S.M., Crisp, J.A., and Spera, F.J.: Long-term volumetric eruption rates and magma budgets: Geochemistry, Geophysics, Geosystems, v. 7, p. 262–266, doi:10.1029/2005GC001002, 2006.

Wijbrans, J.R., Pringle, M.S., Koppers, A.A.P., and Scheveers, R.: Argon geochronology of small samples using the Vulkaan argon laserprobe, *in* Proceedings of the Royal Netherlands Academy of Arts and Sciences, v. 2, p. 185–218, 1995.

York, D.: Least squares fitting of a straight line with correlated errors: Earth and Planetary Science Letters, v. 5, p. 320–324, doi:10.1016/s0012-821x(68)80059-7, 1968.

https://doi.org/10.5194/gchron-2020-30
Preprint. Discussion started: 13 October 2020

Table 1. Previous eruption ages and related stratigraphic units of the island of Milos

Stratigraphy	Sample	Mineral	Location	Petrology	K_2O (wt.%)	Age (Ma)	± 1σ
Unit IV	[1]Angelier_1	Unknown	Fyriplaka	Rhyolite	-	-	-
Unit III	[1]Angelier_2	Unknown	Halepa	Rhyolite	2.44	0.95	0.06
Unit II	[1]Angelier_3	Unknown	Triades	Dacite	1.47	1.71	0.08
	[1]Angelier_4	Unknown	Kleftico	Andesite	1.77	2.33	0.09
	[1]Angelier_5	Unknown	Kleftico	Andesite	1.45	2.50	0.09
Unit I	[1]Angelier_6	Unknown	Adamas	Rhyolite	2.90	2.15	0.08
	[1]Angelier_7	Unknown	Dhemeneghaki	Rhyolite	2.75	1.84	0.08
Phreatic activity	[5]Gif-7358&7359	Carbonized wood	Agia Kiriaki	Lahar deposits	-	200 BC-200 AD	
CFT	[2]M196	Unknown	Fyriplaka	Rhyolite	2.9	0.09	0.02
	[2]M194	Unknown	Fyriplaka	Rhyolite	2.85	0.14	0.03
	[2]M168	Unknown	Trachilas	Rhyolite	3.91	0.37	0.09
	[2]M-48	Biotite	NW of Filiplaka	Rhyolite	6.41	0.48	0.05
PSLD	[3]MI-1	Lava	Plakes	Dacite	2.07	0.80	0.10
	[2]M-OB1	Groundmass	N of Dhemenegaki	Obsidian	2.53	0.88	0.18
	[2]M27	Unknown	Plakes	Dacite	1.87	0.97	0.06
	[3]MI-4	Lava	Plakes	Dacite	2.32	1.20	0.10
	[4]MIL130[e]	Zircon	Triades	Dacite	-	1.44	0.08
	[2]M-OB2	Groundmass	Bombarda	Obsidian	2.73	1.47	0.05
	[6]Fission track1	Groundmass	Adamas	Obsidian	-	1.54	0.18
	[6]Fission track2	Groundmass	Bombarda	Obsidian	-	1.57	0.15
	[7]Fission track3	Groundmass	Bombarda-Adamas	Obsidian	-	1.57	0.12
	[2]M103	Unknown	near Pollonia	Andesite	1.87	1.59	0.25
	[7]Fission track3	Groundmass	Dhemeneghaki	Obsidian	-	1.60	0.06
	[2]M146	Unknown	1km NW of Adamas	Rhyolite	3.09	1.71	0.05
	[2]M110	Unknown	Sarakiniko	Dacite	2.57	1.85	0.10
CDLF	[2]M1	Unknown	Aghios, near Triades	Rhyolite	3.32	2.04	0.09
	[2]M66	Unknown	~1 km NW of Adamas	Dacite	2.61	2.03	0.06
	[4]MIL243[e]	Zircon	Triades	Dacite	-	2.18	0.09
	[2]M156	Unknown	Angathia, near Triades	Dacite	2.84	2.38	0.10
BPS	[4]MIL365[e]	Zircon	Filakopi	Rhyolite	-	2.66	0.07
	[4]MIL343[e]	Zircon	Kalogeros cryptodome	Dacite	-	2.70	0.04
	[2]M164	Unknown	Kleftico	Rhyolite	2.84	3.08	0.08
	[2]M163	Unknown	Kleftico	Andesite	1.18	3.50	0.14

The published ages from 1=Angelier et al. (1977), 2=Fytikas et al. (1976, 1986), 3=Matsuda et al. (1999), 4=Stewart and McPhie (2006), 5=Trainau and Dalabakis (1989), 6=Bigazzi and Radi (1981), Arias et al. (2006). Abbreviations: BPS=Basal pyroclastic series; CDLF=Complex of domes and lava flows; PSLD=Pyroclastic series and lava domes; CTF=Complexes of Trachilas and Fyriplaka. The stratigraphic framework of Stewart and McPhie (2006) is comparable to that of Fytikas et al. (1986). See more details in Fig. 4.

https://doi.org/10.5194/gchron-2020-30
Preprint. Discussion started: 13 October 2020

Table 2. $^{40}Ar/^{39}Ar$ results of incremental heating steps analyses on the Milos volcanic field.

Volcanic Unit	Sample -ID	Irr-ID	Latitude	Age ± 1σ (Ma)	MS WD	$^{39}Ar_K$ (%)	n/ ntotal	$^{40}Ar^*$ (%)	K/Ca ± 1σ	Inverse isochron age (Ma)	$^{40}Ar/^{36}Ar$ ± 1σ	MS WD
Fyriplaka Complex	G15M0 008[B]	VU110-Z22a	36.6729 N 24.4670 E	0.05 ± 0.01	0.04	16.24	3/15	1.20	60.9 ± 10.6	0.05 ± 0.10	298.08 ± 8.77	0.08
		VU110-Z22b		**0.062 ± 0.003**	0.91	71.81	8/11	2.69	57.3 ± 8.4	0.06 ± 0.02	299.39 ± 3.66	1.09
		Combined (Z22)		0.061 ± 0.004	0.82	41.37	11/26	2.29	58.0 ± 6.3	0.07 ± 0.01	296.78 ± 1.78	0.83
	G15M0 012[B]	VU110-Z24a	36.6795 N 24.4828 E	0.05 ± 0.01	3.09	38.89	3/11	2.89	40.0 ± 6.0	0.14 ± 0.03	285.98 ± 4.76	0.07
		VU110-Z24b		0.09 ± 0.02	8.16	48.04	4/11	4.59	30.1 ± 7.1	0.09 ± 0.05	297.46 ± 10.29	12.78
		Combined(Z24)		**0.07 ± 0.01**	7.44	43.53	7/22	3.86	32.3 ± 5.0	0.09 ± 0.03	295.67 ± 7.39	9.02
	G15M0 009[B]	VU110-Z23a	36.6716 N 24.4891 E	0.11 ± 0.02	1.37	18.33	4/12	1.65	45.4 ± 7.3	0.76 ± 0.30	268.52 ± 17.08	0.90
		VU110-Z23b		0.11 ± 0.03	6.77	41.05	4/11	3.13	19.4 ± 3.7	0.29 ± 0.14	285.17 ± 15.80	8.09
		Combined (Z23)		**0.11 ± 0.02**	3.50	29.50	8/21	2.39	19.7 ± 2.6	0.15 ± 0.05	295.78 ± 4.34	4.04
Trachilas Complex	G15M0 007[B]	VU110-Z12a	36.7671 N 24.4124 E	0.30 ± 0.01	4.61	56.50	8/16	14.51	38.3 ± 2.4	0.28 ± 0.05	301.42 ± 9.01	5.47
		VU110-Z12b		**0.317 ± 0.004**	1.29	74.05	4/11	18.30	32.0 ± 2.5	0.31 ± 0.03	299.52 ± 6.40	2.04
		Combined (Z12)		0.31 ± 0.01	5.57	65.27	12/27	15.77	33.1 ± 1.6	0.34 ± 0.03	293.05 ± 5.50	5.84
Kontaro dome	G15M0 020[G]	VU108-Z5a_5	36.7234 N 24.3952 E	1.52 ± 0.01	1.06	61.82	8/12	18.30	1.51 ± 0.05	1.49 ± 0.02	300.03 ± 0.86	0.95
		VU108-Z5b_1		1.56 ± 0.01	1.94	41.54	3/10	47.94	1.73 ± 0.06	1.58 ± 0.02	294.97 ± 3.74	2.17
		VU108-Z5b_2		1.52 ± 0.01	1.73	62.45	5/10	22.95	1.56 ± 0.08	1.53 ± 0.02	298.12 ± 0.89	2.34
		Combined (Z5)		**1.54 ± 0.01**	3.06	57.32	16/32	25.31	1.58 ± 0.04	1.55 ± 0.01	297.41 ± 0.57	2.82
	G15M0 019[G]	VU108-Z6a_4	36.7211 N 24.3950 E	1.62 ± 0.01	3.80	89.75	9/11	34.28	0.91 ± 0.05	1.62 ± 0.02	297.66 ± 1.36	4.40
		VU108-Z6a_5		1.55 ± 0.01	4.50	95.41	10/12	35.26	0.88 ± 0.06	1.55 ± 0.01	298.73 ± 1.29	5.40
		VU108-Z6b_1		1.56 ± 0.01	4.05	56.64	4/10	53.19	1.02 ± 0.01	**1.48 ± 0.02**	315.46 ± 5.20	0.44
		Combined (Z6)		1.55 ± 0.01	32.15	80.97	27/45	38.78	0.93 ± 0.04	1.53 ± 0.02	300.60 ± 2.27	34.25
Dheme--neghaki volcano	G15M0 032B[O]	VU108-Z18	36.7084 N 24.5324 E	**1.825 ± 0.002**	0.91	98.64	12/13	93.86	1.83 ± 0.04	1.825±0.003	301.52 ± 3.34	0.93
Triades lava dome	G15M0 021[B]	VU110-Z4_2	36.7402 N 24.3397 E	**1.97 ± 0.01**	1.66	63.83	4/12	54.72	107.55 ± 20.64	1.97 ± 0.03	299.16 ± 5.36	2.56
		VU110-Z4_2b		2.01 ± 0.01	6.76	75.39	6/16	57.84	54.43 ± 8.29	2.04 ± 0.05	293.08 ± 10.44	8.15
		Combined (Z4)		1.99 ± 0.01	9.08	69.12	10/28	56.59	73.52 ± 6.46	2.00 ± 0.04	295.64 ± 7.89	10.30
Adamas lava dome	G15M0 004[A]	VU108-Z10_1	36.7282 N 24.4315 E	2.99 ± 0.11	1.00	87.31	4/12	16.36	0.030 ± 0.002	7.89 ± 2.46	202.39 ± 48.47	0.01
		VU108-Z10_2		2.86 ± 0.09	1.50	86.18	7/11	17.58	0.029 ± 0.002	0.70 ± 0.29	348.91 ± 27.33	1.00
		Combined (Z10)		2.90 ± 0.07	1.31	86.74	11/23	17.13	0.029 ± 0.001	**1.95 ± 0.45**	319.51 ± 14.70	1.17
The dyke of Mavro Vouni lava dome	G15M0 016[G]	VU108-Z8a	36.6668 N 24.3398 E	2.71 ± 0.02	2.31	79.64	8/12	16.57	0.24 ± 0.05	2.65 ± 0.10	299.84 ± 2.32	2.92
		VU108-Z8a_4		2.61 ± 0.03	0.93	57.41	7/12	16.86	0.12 ± 0.07	2.69 ± 0.10	296.44 ± 2.49	0.69
		VU108-Z8b_1		2.67 ± 0.01	1.50	65.57	7/11	17.25	0.11 ± 0.04	2.55 ± 0.05	301.53 ± 1.14	0.71
		Combined (Z8)		**2.66 ± 0.01**	2.51	67.27	22/35	16.87	0.14 ± 0.02	2.61 ± 0.05	300.01 ± 1.18	2.78
Korokia dome	G15M0 029[G]	VU108-Z16a	36.7465 N 24.5200 E	2.67 ± 0.01	0.96	23.61	4/13	56.34	0.53 ± 0.05	2.68 ± 0.02	296.64 ± 3.18	1.25
		VU108-Z16b_1		2.69 ± 0.01	1.32	27.08	3/13	55.78	0.55 ± 0.04	2.67 ± 0.03	301.16 ± 4.72	2.13
		Combined (Z16)		2.68 ± 0.01	1.66	25.30	7/26	56.10	0.54 ± 0.03	2.67 ± 0.02	300.00 ± 2.94	1.98
Coherent dacite of Profitis Illias volcano	G15M0 015[G]	VU108-Z9a	36.6629 N 24.3596 E	3.12 ± 0.02	9.07	43.07	3/12	42.73	1.31 ± 0.05	3.06 ± 0.02	304.19 ± 1.25	0.01
		VU108-Z9b_1		2.98 ± 0.02	4.53	27.00	4/14	39.35	0.98 ± 0.06	3.04 ± 0.02	293.83 ± 1.38	1.14
		Combined (Z9)		2.99 ± 0.02	5.54	22.79	6/26	41.77	1.00 ± 0.04	**3.06 ± 0.02**	292.77 ± 1.62	1.90
Coherent dacite of Profitis Illias volcano	G15M0 017[G]	VU108-Z7a	36.6596 N 24.3675 E	**3.64 ± 0.08**	3.13	28.62	7/13	9.77	1.04 ± 0.02	4.14 ± 0.49	293.87 ± 4.77	3.44
		VU108-Z7a_4		**4.10 ± 0.06**	2.13	34.71	6/17	9.08	1.10 ± 0.01	4.11 ± 1.40	298.44 ± 15.51	3.24
		VU108-Z7b_1		**3.41 ± 0.05**	3.95	31.41	5/13	9.95	1.00 ± 0.03	3.68 ± 0.71	295.97 ± 7.34	7.09
		Combined (Z7)		3.63 ± 0.08	14.04	31.40	18/43	9.59	1.04 ± 0.02	2.19 ± 0.32	311.31 ± 3.60	10.19

The age in bold is considered as the best estimate of the eruptive age.

$^{40}Ar^*$ (%) is average radiogenic ^{40}Ar in analyses included in the weighted mean.

The experiment was analyzed on biotite[B], obsidian[O], amphibole[A] and groundmass[G] of sample.

Same steps were used for the calculation of isochron ages as used in the weighted mean ages.

https://doi.org/10.5194/gchron-2020-30
Preprint. Discussion started: 13 October 2020

Table 3. $^{40}Ar/^{39}Ar$ results of single grain fusion analyses on the Milos volcanic field.

Volcanic unit	Sample-ID	Irr-ID	Location	Age ± 1σ (Ma)	MS WD	$^{39}Ar_K$ (%)	n/ ntotal	$^{40}Ar^*$ (%)	K/Ca ± 1σ	Inverse isochron age (Ma)	$^{40}Ar/^{36}Ar$ ± 1σ	MS WD
Fyriplaka complex	G15M0008[B]	VU110-Z22	36.6729 N 24.4670 E	0.71 ± 0.06	0.41	25.78	8/23	8.67	17.5 ± 1.8	0.64 ± 0.20	302.75 ± 12.62	0.46
	G15M0012[B]	VU110-Z24	36.6795 N 24.4828 E	1.12 ± 0.11	2.26	60.49	14/23	7.32	14.9 ± 0.8	0.26 ± 0.07	316.75 ± 19.49	2.29
	G15M0009[B]	VU110-Z23	36.6716 N 24.4891 E	0.65 ± 0.07	1.16	79.91	19/23	5.87	12.0 ± 0.5	0.28 ± 0.07	309.57 ± 16.01	1.22
Trachilas complex	G15M0007[B]	VU110-Z12	36.7671 N 24.4124 E	0.47 ± 0.05	0.75	72.65	15/22	9.09	14.8 ± 0.5	0.55 ± 0.12	293.95 ± 11.30	0.80
Kalamos lava	G15M0033[B]	VU108-Z19	36.6662 N 24.4652 E	**0.412 ± 0.004**	1.10	77.24	8/10	22.22	20.5 ± 2.7	0.39 ± 0.02	303.32 ± 3.06	0.89
Trachilas complex	G15M0034[B]	VU108-Z20	36.7550 N 24.4244 E	**0.51 ± 0.02**	0.95	56.92	6/10	3.53	13.7 ± 1.2	0.61 ± 0.08	296.45 ± 1.65	0.92
	G15M0035[B]	VU108-Z21	36.7550 N 24.4244 E	**0.63 ± 0.02**	1.26	73.43	6/9	4.87	17.7 ± 1.1	0.77 ± 0.13	294.99 ± 3.17	1.42
Halepa lava dome	G15M0013[B]	VU108-Z13	36.6716 N 24.4406 E	**1.04 ± 0.01**	1.62	82.40	9/10	26.30	*15.2 ± 0.2	1.02 ± 0.04	299.77 ± 4.06	0.00
Triades lava dome	G15M0021[B]	VU110-Z4	36.7402 N 24.3397 E	2.48 ± 0.04	1.49	87.08	4/12	36.09	13.00± 0.60	3.44 ± 0.46	228.58 ± 36.66	1.39
	G15M0022[B]	VU108-Z14	36.7402 N 24.3397 E	**2.10 ± 0.01**	1.37	100.00	10/10	36.04	*11.7 ± 0.2	2.08 ± 0.06	299.44 ± 4.63	1.59
	G15M0023[B]	VU108-Z3	36.7263 N 24.3420 E	**2.10 ± 0.01**	1.72	55.58	6/11	35.93	*76.1 ± 2.4	2.13 ± 0.06	296.12 ± 4.63	2.08
	G15M0024[B]	VU108-Z15	36.7277 N 24.3415 E	**2.13 ± 0.01**	0.46	63.67	6/10	29.74	22.5 ± 3.2	2.09 ± 0.03	300.50 ± 1.58	0.23
Mavros Kavos lava dome	G15M0025[B]	VU108-Z2	36.6876 N 24.3515 E	**2.36 ± 0.01**	0.70	84.62	9/10	37.62	43.2 ± 2.7	2.34 ± 0.04	300.57 ± 3.49	0.78
	G15M0026[B]	VU108-Z1b	36.6848 N 24.3500 E	2.35 ± 0.01	1.36	95.23	9/10	38.56	12.8 ± 2.3	**2.42 ± 0.04**	292.01 ± 2.92	0.93
Kalegeros crypto-dome	G15M0006[B]	VU108-Z11	36.7643 N 24.5157 E	2.72 ± 0.01	1.95	87.67	9/10	47.90	*28.3 ± 0.5	**2.62 ± 0.04**	310.21 ± 4.04	0.99

The age in bold is considered as the best estimate of the eruptive age.

$^{40}Ar^*$ (%) is average radiogenic ^{40}Ar in analyses included in the weighted mean.

*The K/Ca ratio is calibrated by removing the step with excess ^{37}Ar (Ca) (>1).

[B]The experiment was analyzed on biotite of sample.

Same steps were used for the calculation of isochron ages as used in the weighted mean ages.

https://doi.org/10.5194/gchron-2020-30
Preprint. Discussion started: 13 October 2020

Table 4. Major-element composition of volcanic samples from the Milos Volcanic Field.

Sample-ID	Rock Types	SiO_2 wt.%	TiO_2 wt.%	Al_2O_3 wt.%	Fe_2O_3T wt.%	MnO wt.%	MgO wt.%	CaO wt.%	Na_2O wt.%	K_2O wt.%	P_2O_5 wt.%	BaO wt.%	LOI. wt.%
G15M0008	Pumice	76.71	0.14	12.96	1.11	0.058	0.22	1.27	4.04	3.22	0.021	0.056	0.16
G15M0012	Pumice	75.47	0.13	12.77	1.08	0.057	0.22	1.27	4.12	3.15	0.024	0.055	0.35
G15M0009	Pumice	76.02	0.13	12.91	1.04	0.059	0.23	1.19	3.99	3.41	0.022	0.056	0.16
G15M0007	Pumice	76.68	0.08	12.60	0.85	0.084	0.11	0.75	3.58	4.74	0.009	0.051	0.17
G15M0033	Rhyolite	76.68	0.10	12.86	0.88	0.087	0.18	0.85	3.71	4.46	0.014	0.045	0.14
G15M0034	Pumice	76.89	0.08	12.64	0.84	0.085	0.11	0.74	3.50	4.85	0.009	0.050	0.33
G15M0035	Pumice	78.40	0.08	12.93	0.85	0.087	0.11	0.76	3.49	4.95	0.010	0.052	0.06
G15M0013	Rhyolite	72.87	0.22	14.11	1.95	0.071	0.51	2.23	3.73	3.43	0.044	0.055	0.13
G15M0020	unknown	-	-	-	-	-	-	-	-	-	-	-	-
G15M0019	Dacite	64.26	0.56	16.08	5.33	0.112	2.42	5.33	3.60	1.69	0.038	0.038	0.09
G15M0032 B	Obsidian	75.57	0.20	13.32	1.46	0.062	0.33	1.71	3.95	3.26	0.033	0.055	0.07
G15M0004	Dacite	63.56	0.57	16.09	5.70	0.114	2.81	6.01	3.49	1.57	0.090	0.036	0.04
G15M0021	Trachy-dacite	64.98	0.35	16.82	3.69	0.075	1.50	2.19	2.61	7.24	0.049	0.353	0.17
G15M0022	Enclave	53.87	0.60	19.91	7.61	0.157	3.93	5.45	1.73	6.11	0.075	0.34	0.21
G15M0023	Rhyolite	73.05	0.29	14.24	3.23	0.017	0.53	2.35	3.28	3.36	0.043	0.064	0.12
G15M0024	Rhyolite	76.57	0.23	11.73	1.69	0.025	0.46	2.36	2.85	2.31	0.045	0.046	0.20
G15M0025	Rhyodacite	69.56	0.42	15.30	3.15	0.106	0.88	3.67	3.49	2.98	0.105	0.059	0.19
G15M0026	Rhyodacite	69.57	0.43	16.08	3.38	0.037	0.62	3.43	3.56	2.63	0.087	0.061	0.09
G15M0006	Rhyodacite	68.58	0.40	15.90	2.67	0.074	0.81	2.89	4.19	3.61	0.108	0.099	0.12
G15M0016	Basaltic Andesite	55.72	0.66	18.43	7.70	0.135	4.42	8.78	2.90	1.41	0.090	0.030	0.06
G15M0029	Dacite	61.91	0.79	17.09	5.90	0.087	1.84	6.07	3.57	2.71	0.200	0.126	0.09
G15M0015	Andesite	63.77	0.64	16.33	5.42	0.097	2.48	5.91	3.35	1.91	0.089	0.036	0.04
G15M0017	Dacite	68.03	0.58	15.90	3.47	0.066	1.34	4.31	3.76	2.69	0.101	0.044	0.48

The classification of rock type for each sample is on the basis of field observation and SiO_2 versus K_2O plot of Le Bas et al. (1986). All iron expressed as Fe_2O_3T(otal).

https://doi.org/10.5194/gchron-2020-30
Preprint. Discussion started: 13 October 2020

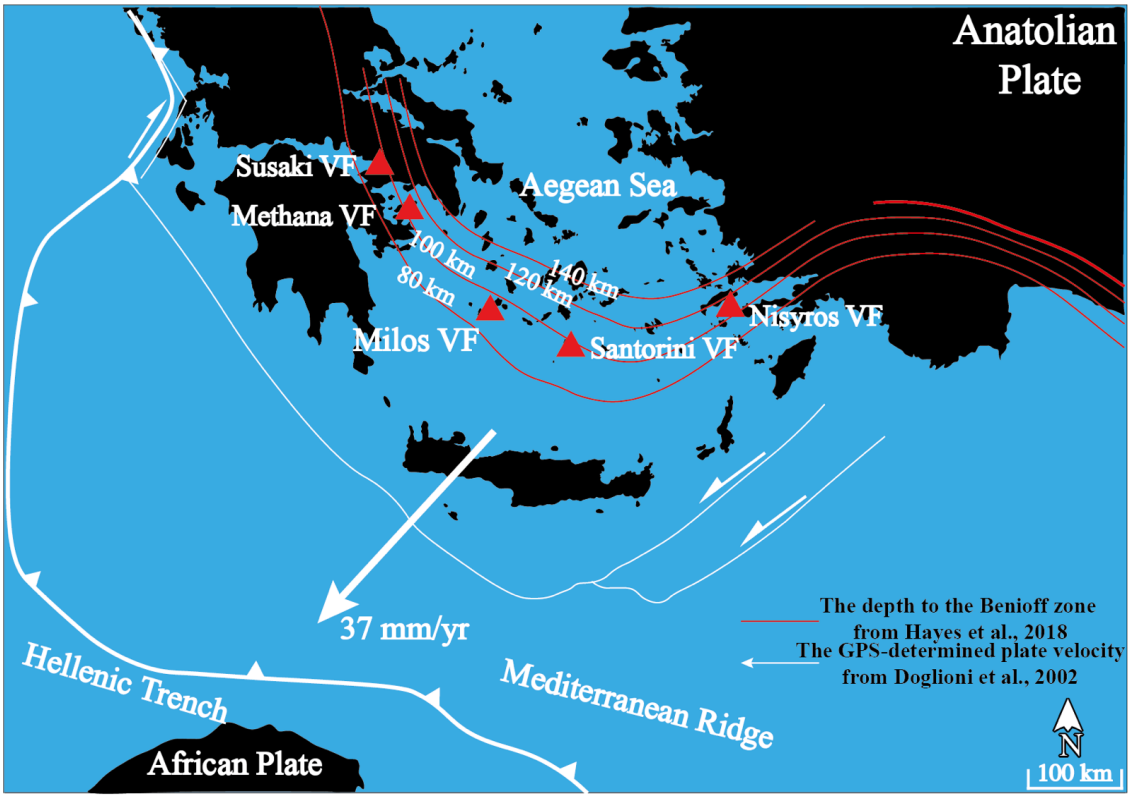

Figure 1. Map of the South Aegean Volcanic Arc (SAVA); active volcanic fields (VF) are indicated by red triangles: Methana and Milos VFs in the western SAVA, Santorini VF in the centre and Nisyros VF in the eastern SAVA.

https://doi.org/10.5194/gchron-2020-30
Preprint. Discussion started: 13 October 2020

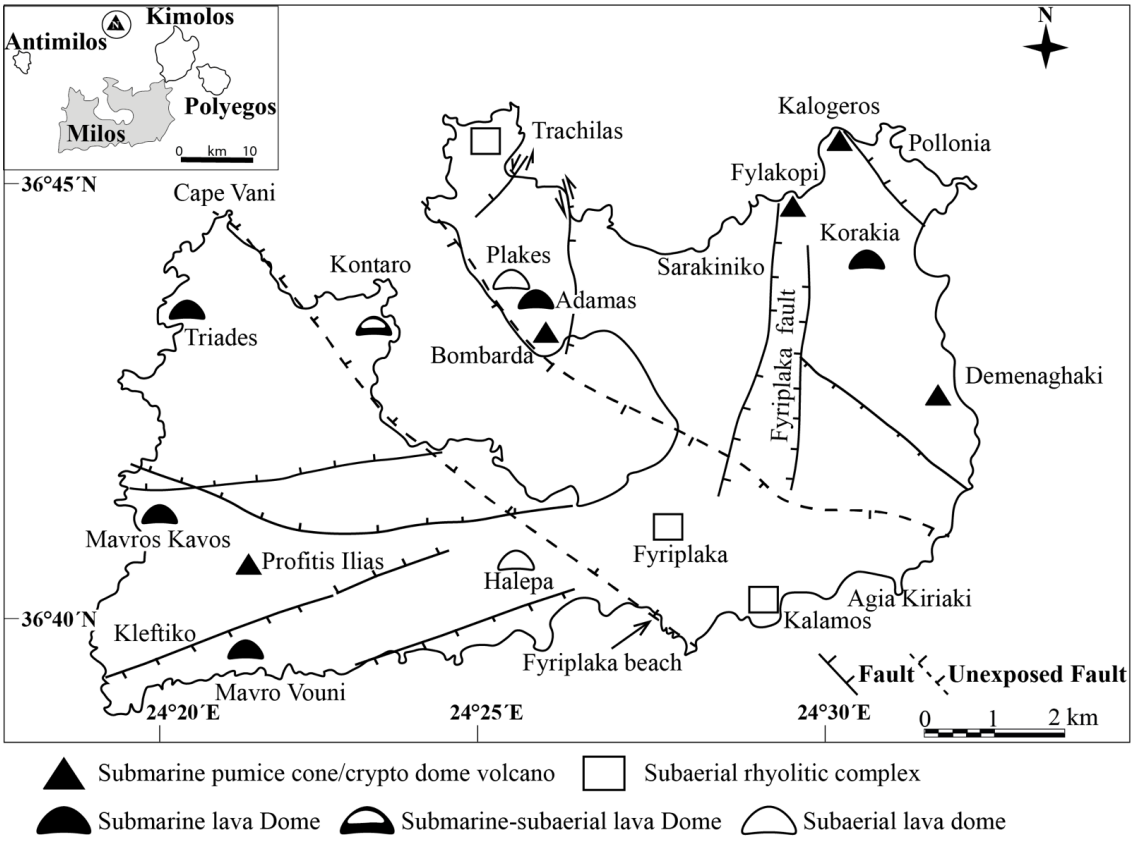

Figure 2. Locations of the submarine pumice cone/crypto dome volcanoes, submarine, submarine-subaerial and subaerial domes and rhyolitic complexes (tuff cone and associated lava) of Milos, modified after Fytikas et al. (1986) and Stewart and McPhie (2006). The volcano types are according to Stewart and McPhie (2006).

https://doi.org/10.5194/gchron-2020-30
Preprint. Discussion started: 13 October 2020

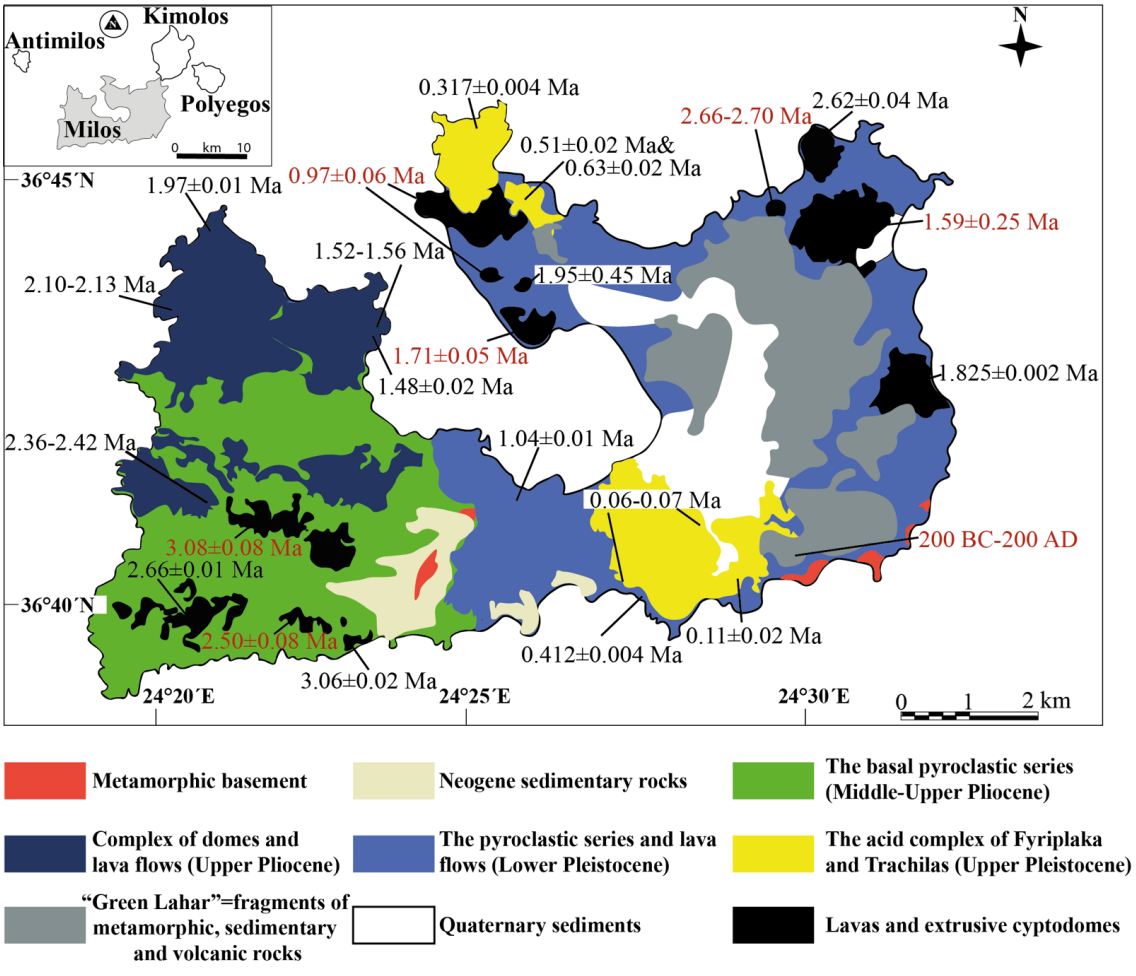

Figure 3. Simplified geological map of Milos with our $^{40}Ar/^{39}Ar$ ages of key volcanic deposits, modified after Stewart and McPhie (2006) and Grasemann et al. (2018). The stratigraphic units of Milos are from Fytikas et al. (1986). Age data from this study are in black, published ages are shown in red (Fytikas et al., 1986, Traineau and Dalabakis, 1989, Van Hinsbergen et al., 2004 and Stewart and McPhie, 2006).

https://doi.org/10.5194/gchron-2020-30
Preprint. Discussion started: 13 October 2020

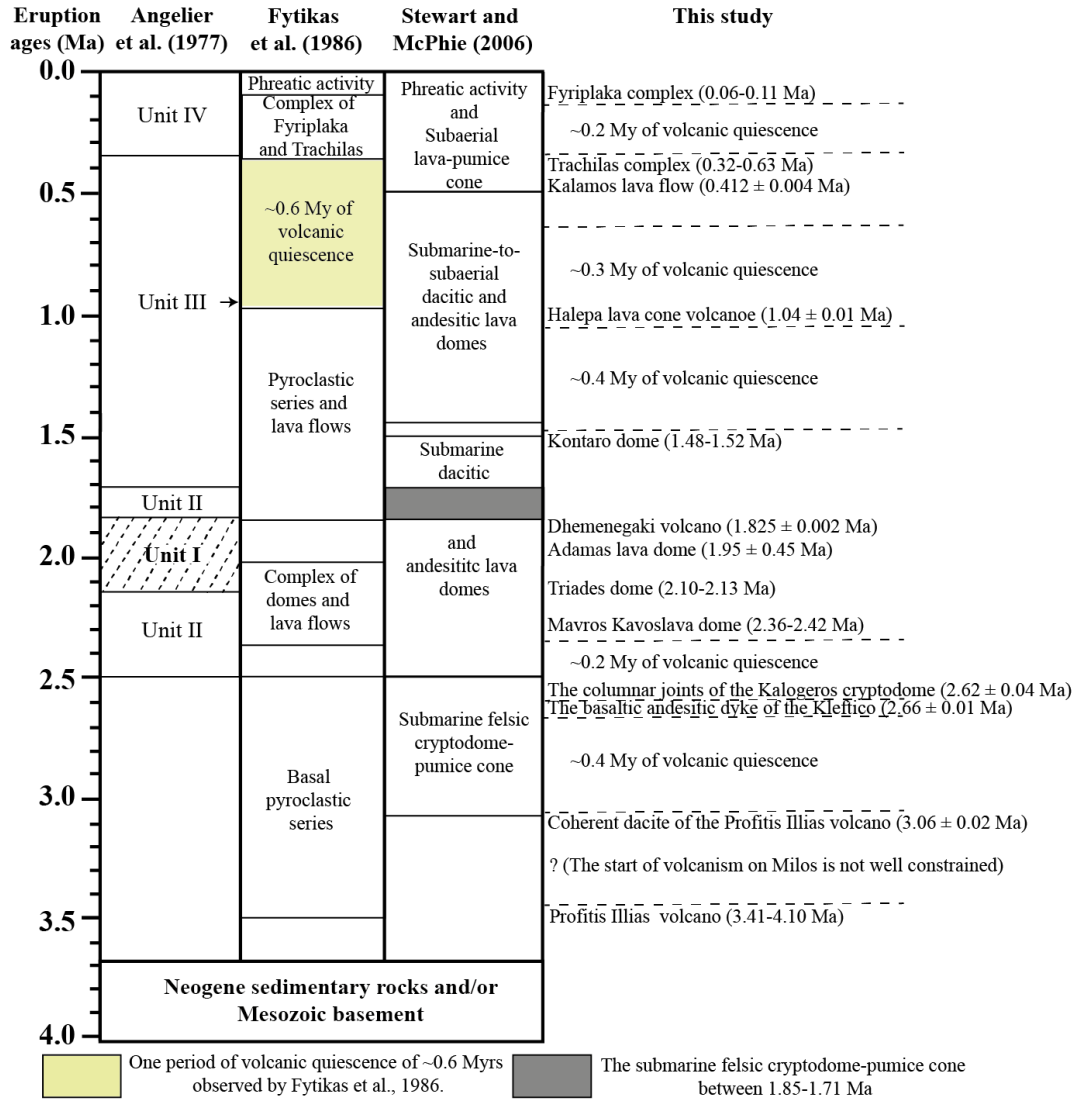

Figure 4. Previous proposed stratigraphy of Milos and $^{40}Ar/^{39}Ar$ results of this study. Volcanic unit II of Angelier et al. (1977) contains unit I. Stewart and McPhie (2006) described the volcanic faces of Milos mainly based on the geochronological works of Angelier et al. (1977) and Fytikas et al. (1986).

https://doi.org/10.5194/gchron-2020-30
Preprint. Discussion started: 13 October 2020

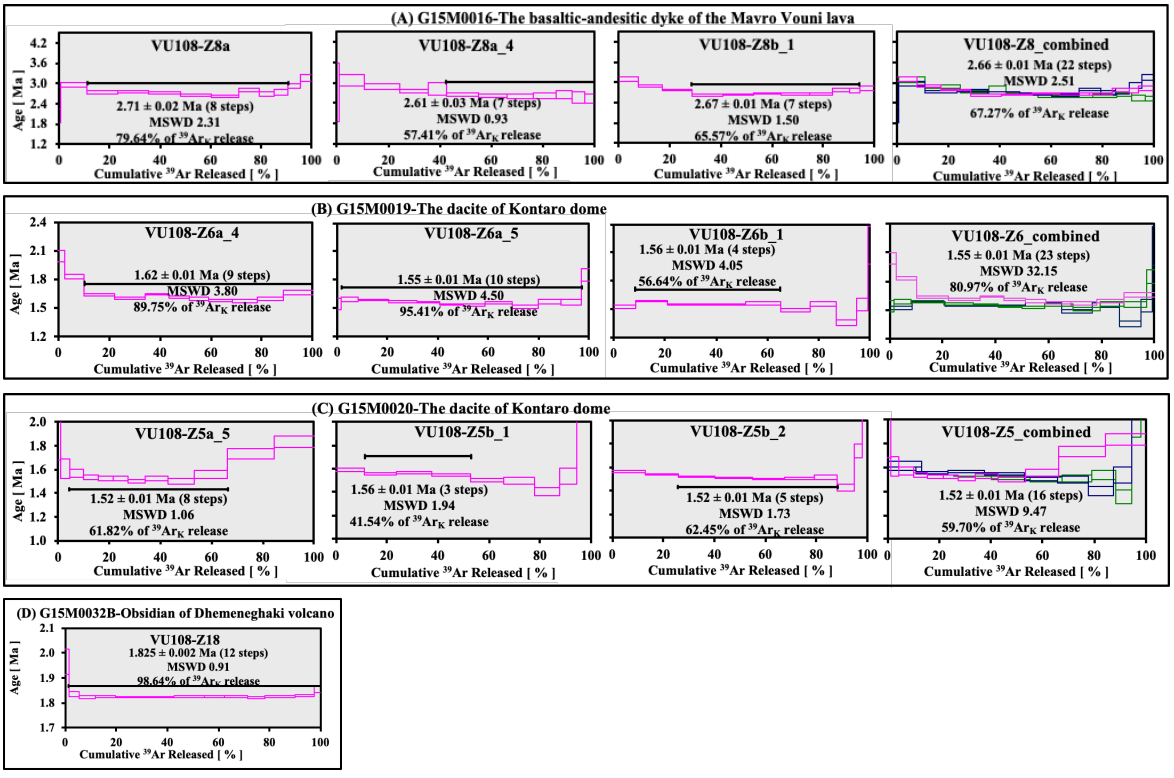

Figure 5. Groundmass $^{40}Ar/^{39}Ar$ plateau ages for samples G15M0016 (A), G15M0019 (B), G15M0020 (C) and G15M0032B (D). Individual steps and final age calculation are reported with 1σ errors. The Mavro Vouni lava dome (A), Kontaro dacitic dome (B, C) and Dhemeneghaki volcano (D) are located in respectively the south-western, north-eastern and eastern parts of Milos VF.

https://doi.org/10.5194/gchron-2020-30
Preprint. Discussion started: 13 October 2020

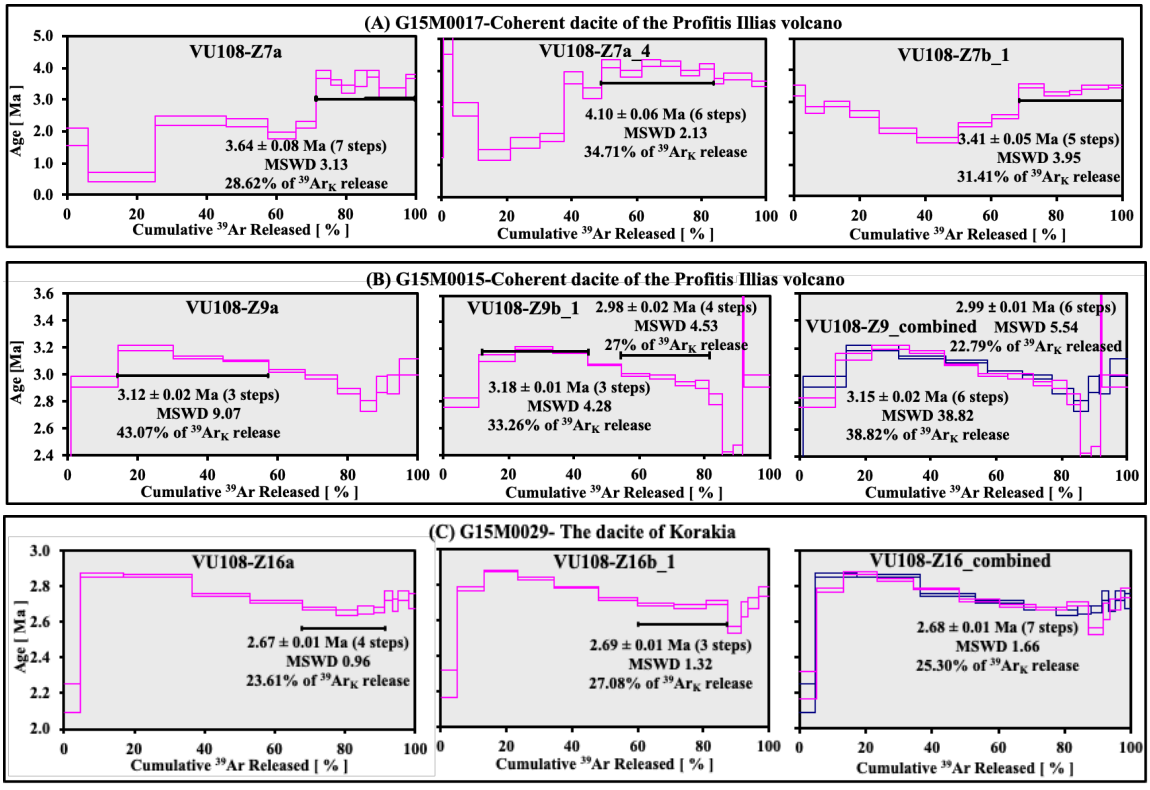

Figure 6. Groundmass $^{40}Ar/^{39}Ar$ plateau ages for samples G15M0017 (A), G15M0015 (B) and G15M0029 (C). Individual steps and final age calculation are reported with 1σ errors. The Profitis Illias volcano (A, B) and dacitic Korakia dome (C), respectively, are located in the south-western and north-eastern parts of Milos VF.

https://doi.org/10.5194/gchron-2020-30
Preprint. Discussion started: 13 October 2020

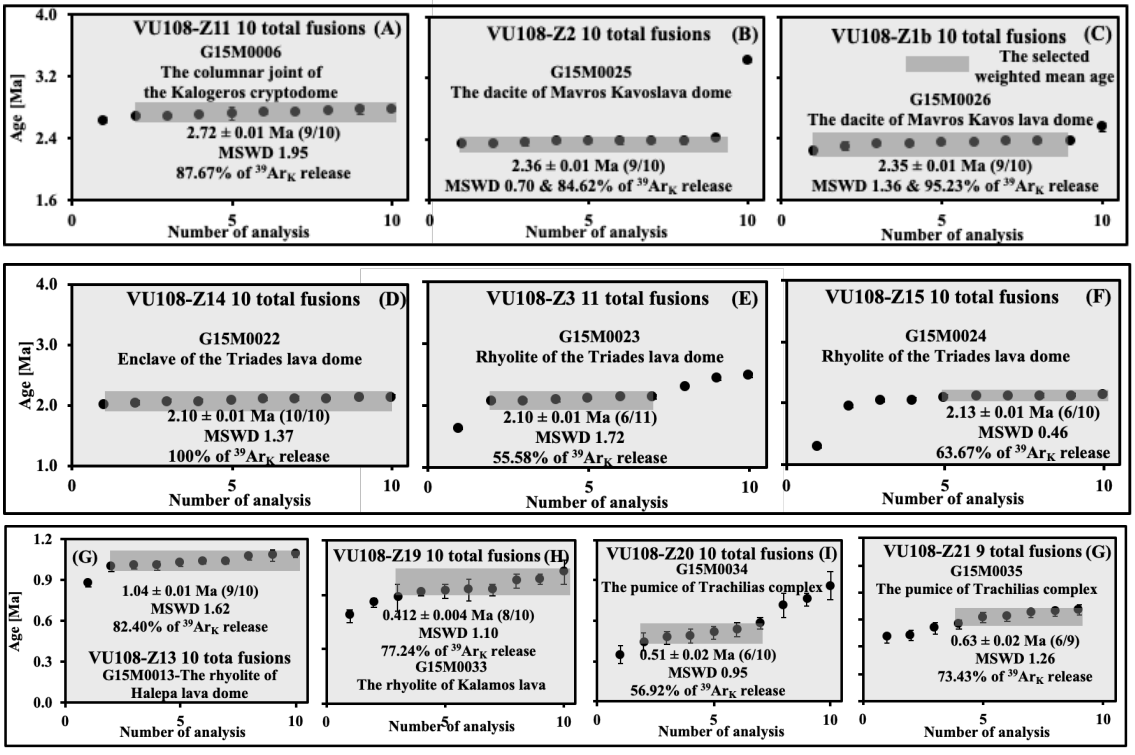

Figure 7. Biotite $^{40}Ar/^{39}Ar$ total fusion ages for samples G15M0006 (A) and G15M0025-26(B, C), G15M0022-24 (D-F), G15M0013 (G) and G15M0033-35 (H-G). Data outside shaded area are not included in the weighted mean. Individual steps and final age calculation are reported with 1σ errors. The Kalogeros cryptodome and Mavros Kavoslava dome are located in, respectively, the north-eastern and south-western parts of Milos VF. Triades lava dome, Halepa lava dome, Trachilias complex and the Kalamos lava, respectively, were found in the southern, northern and south-eastern parts of Milos VF.

https://doi.org/10.5194/gchron-2020-30
Preprint. Discussion started: 13 October 2020

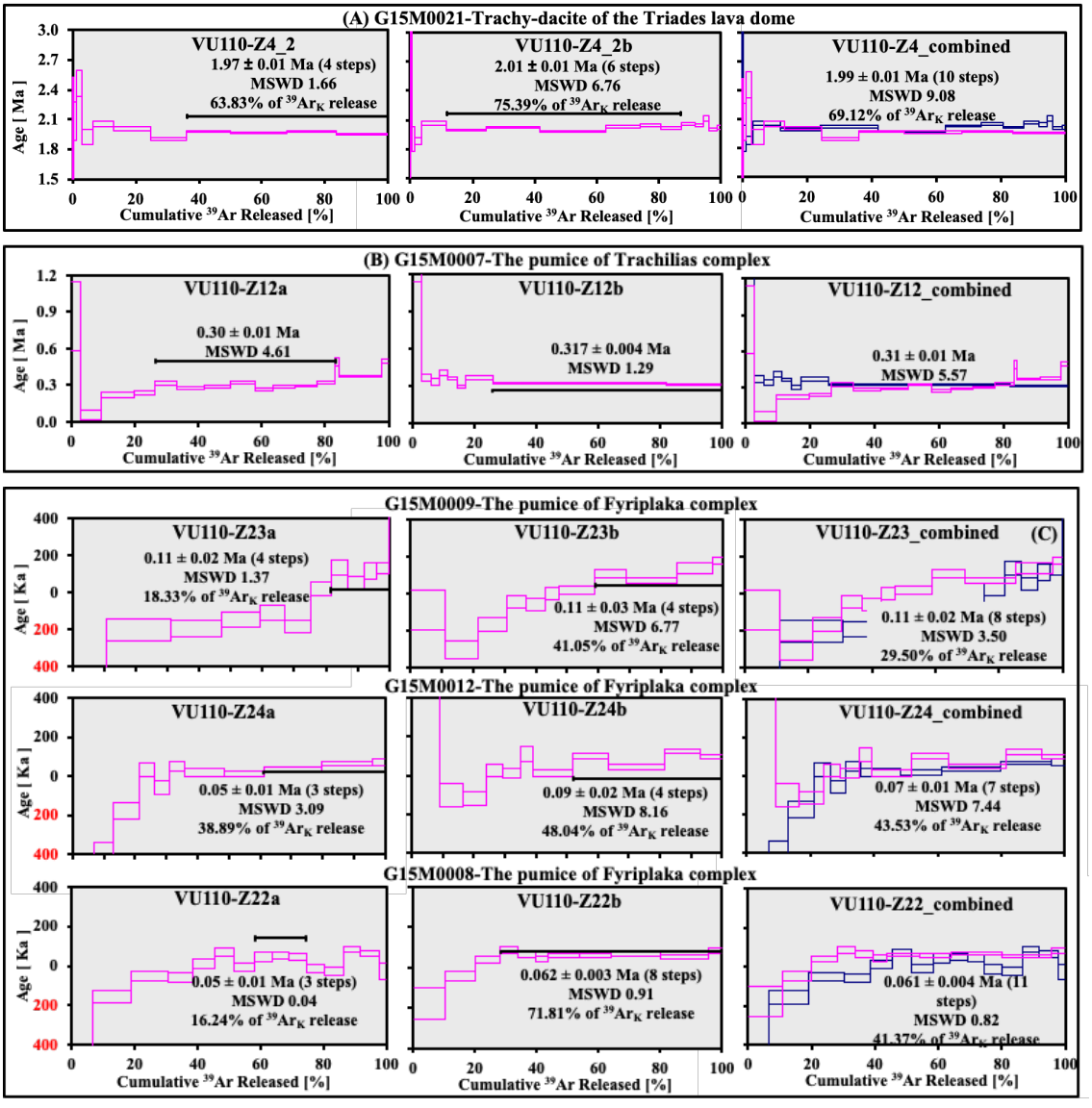

Figure 8. Biotite $^{40}Ar/^{39}Ar$ plateau ages for samples G15M0021 (A), G15M0007 (B), and G15M0009 (VU110-Z23a, 23b and 23_combined), G15M0012 (VU110-24a, 24b and Z24_combined) and G15M0008 (VU110-Z22a, Z22b and Z22_combined) (C). The numbers in red represent negative ages. Individual steps and final age calculation are reported with 1σ errors. The Triades lava dome, Trachilias and Fyriplaka complexes, respectively, locate in the north-western, northern and south-eastern parts of Milos VF.

https://doi.org/10.5194/gchron-2020-30
Preprint. Discussion started: 13 October 2020

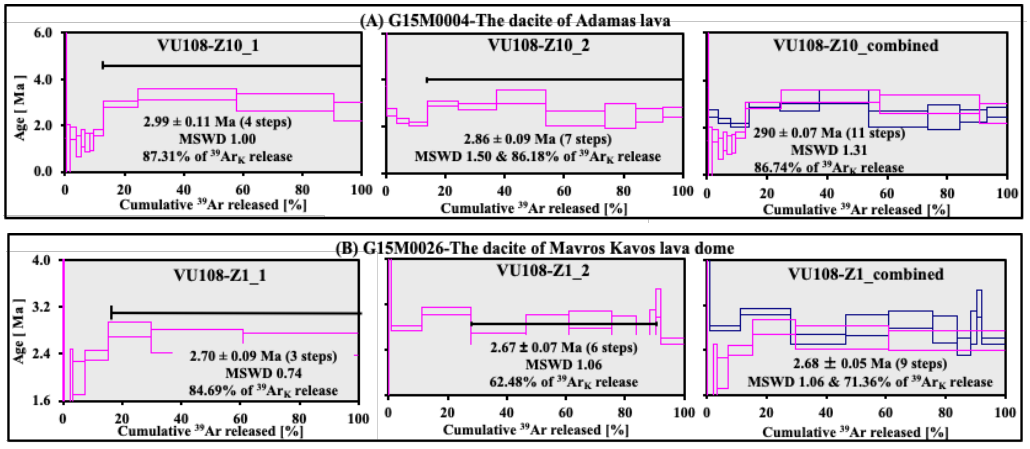

Figure 9. Amphibole $^{40}Ar/^{39}Ar$ plateau ages for samples G15M0004 (A) and G15M0026 (B). Individual steps and final age calculation are reported with 1σ errors. The Adamas and Mavros Kavos lava domes, respectively, are located in the northern and south-western parts of Milos VF.

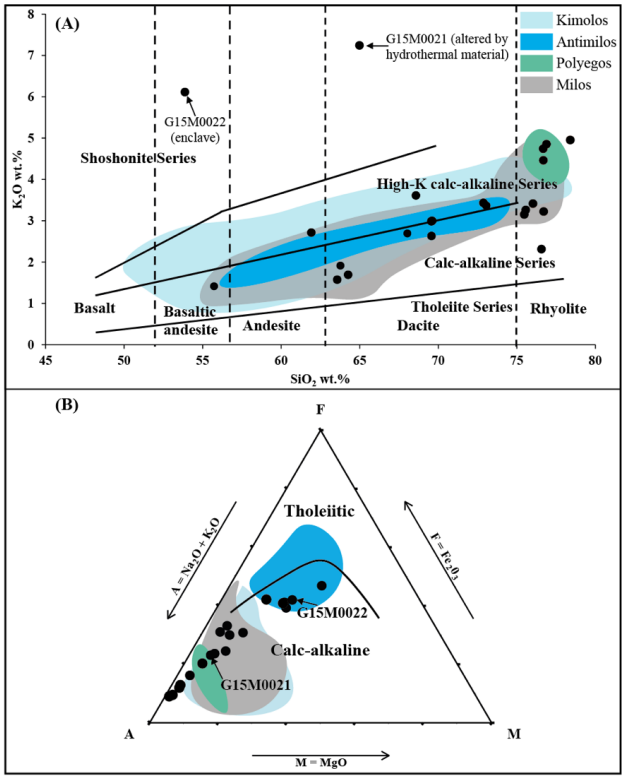

Figure 10. SiO_2 versus K_2O (A) and AFM (B) diagrams for the Milos volcanic field with data of this study as solid circles. Published data are represented by shaded fields (Francalanci and Zelmer, 2019 and reference therein). Fields for the tholeiite, calc-alkaline, high-K calc-alkaline and shoshonitic series are from Peccerillo and Taylor (1976). Vertical lines defining fields for basalt, basaltic-andesite, andesite, dacite and rhyolite are from Bas et al. (1986). The solid line dividing tholeiitic and calc-alkaline fields is from Irvine and Baragar (1971).

https://doi.org/10.5194/gchron-2020-30
Preprint. Discussion started: 13 October 2020

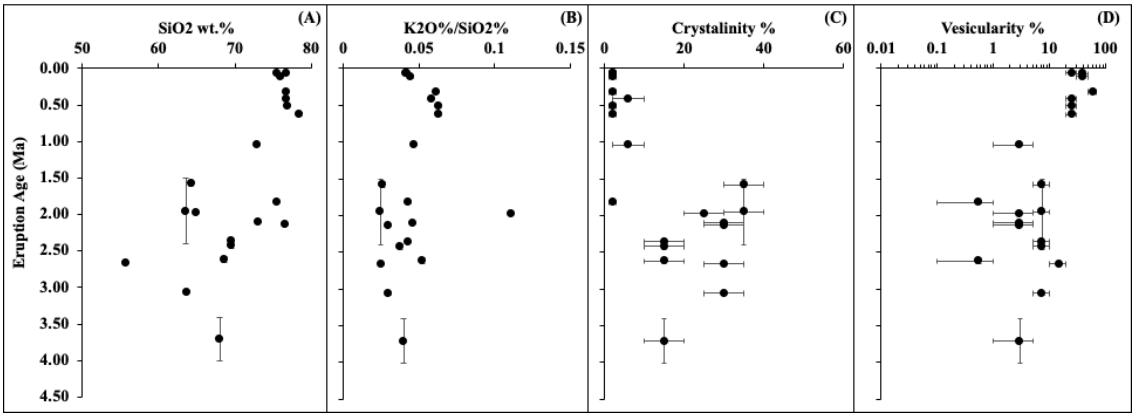

Figure 11. Eruption age versus (A) SiO_2 wt.%, (B) $K_2O\%/SiO_2\%$, (C) Crystallinity % and (D) Vesicularity % of Milos volcanic units of this study. The estimations of crystallinity and vesicularity on the older samples (>1.0 Ma) are all from lava and domes. The younger samples (<1.0 Ma) are pumiceous pyroclastic units. Data of the old pumices of the Profitis Illias (~3.08 Ma) and Filakopi volcanoes (2.66 Ma) are lacking due to the severe alteration.

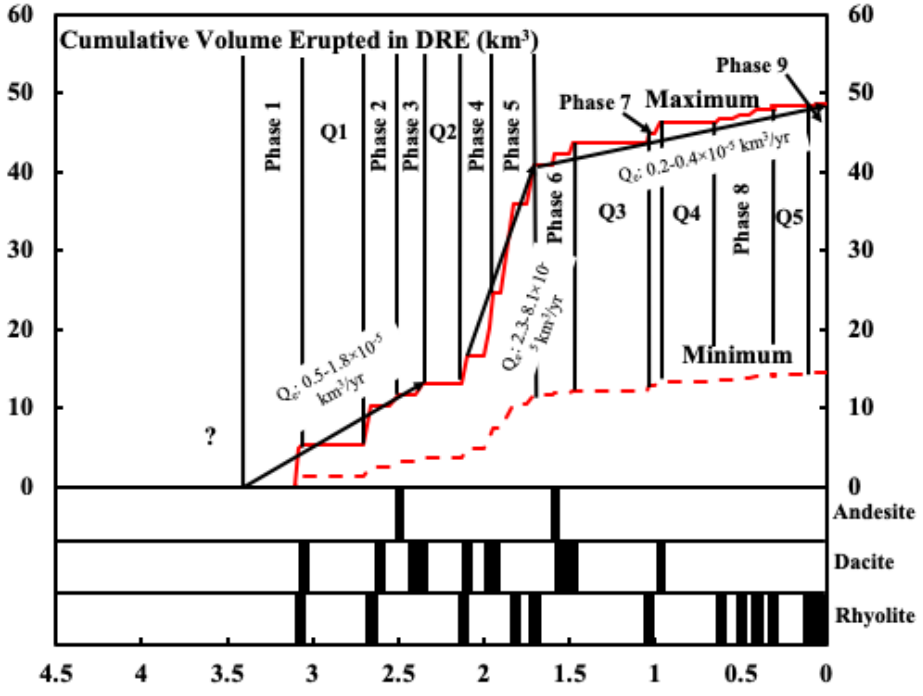

Figure 12. Cumulative eruption volume versus time for the volcanic deposits of Milos. The maximum (Max; red line) and minimum (Min; dashed red line) cumulative eruption volume curves were estimated from Campos et al. (1996) and Stewart and McPhie (2006); see discussion for more details. In the lower part of the figure the composition of the erupted products is shown (data from this study and Fytikas et al., 1986). The exact volume of volcanic products between 4.1 and 3.06 Ma is not well constraint and indicated with a question mark. Note the shift to more felsic compositions over time and the decrease in erupted volumes after 1.6 Ma. Q1-5 are the four periods of volcanic quiescence that lasted more than 200 kyr. Q_e is the long term volumetric volcanic output rate explained in discussion.

https://doi.org/10.5194/gchron-2020-30
Preprint. Discussion started: 13 October 2020

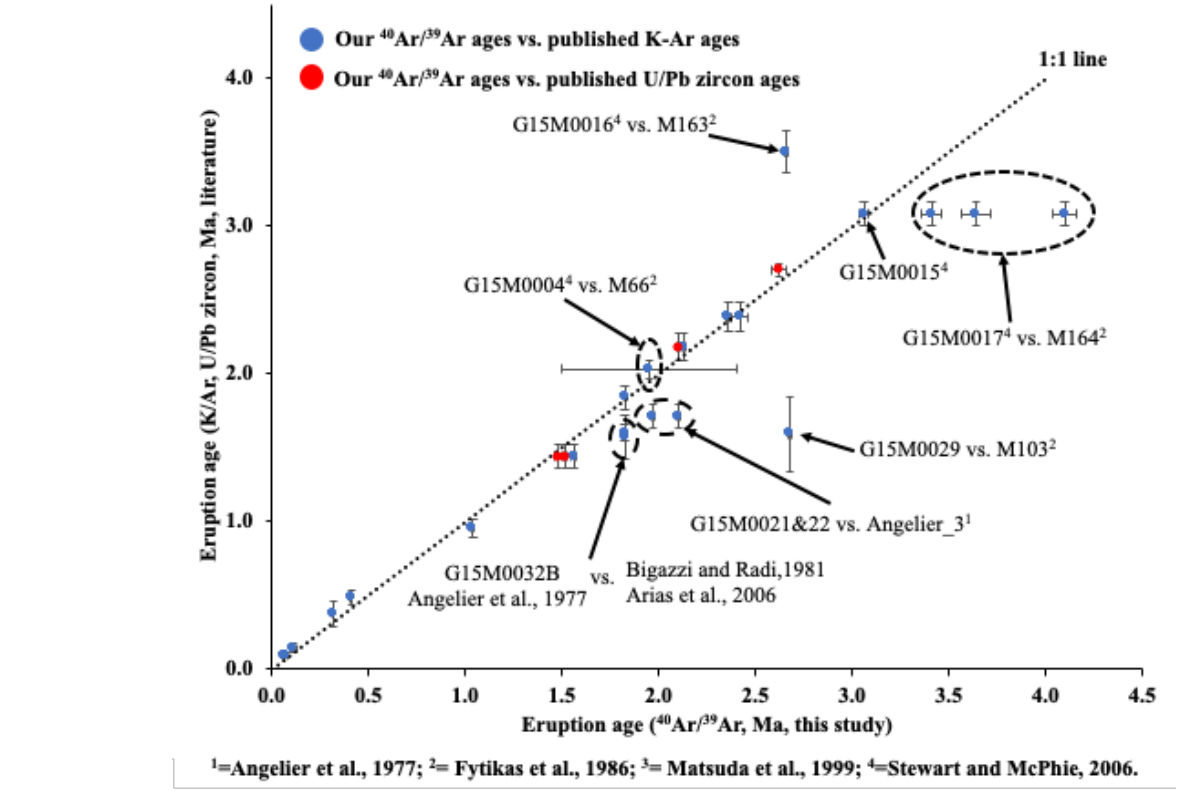

[1]=Angelier et al., 1977; [2]= Fytikas et al., 1986; [3]= Matsuda et al., 1999; [4]=Stewart and McPhie, 2006.

Figure 13. The $^{40}Ar/^{39}Ar$ ages of this study compared to the K/Ar ages and U/Pb zircon ages for the same volcanic units. The number in the sample names of Angelier indicates the location number given in Angelier et al. (1977, their Fig. 3).

https://doi.org/10.5194/gchron-2020-30
Preprint. Discussion started: 13 October 2020

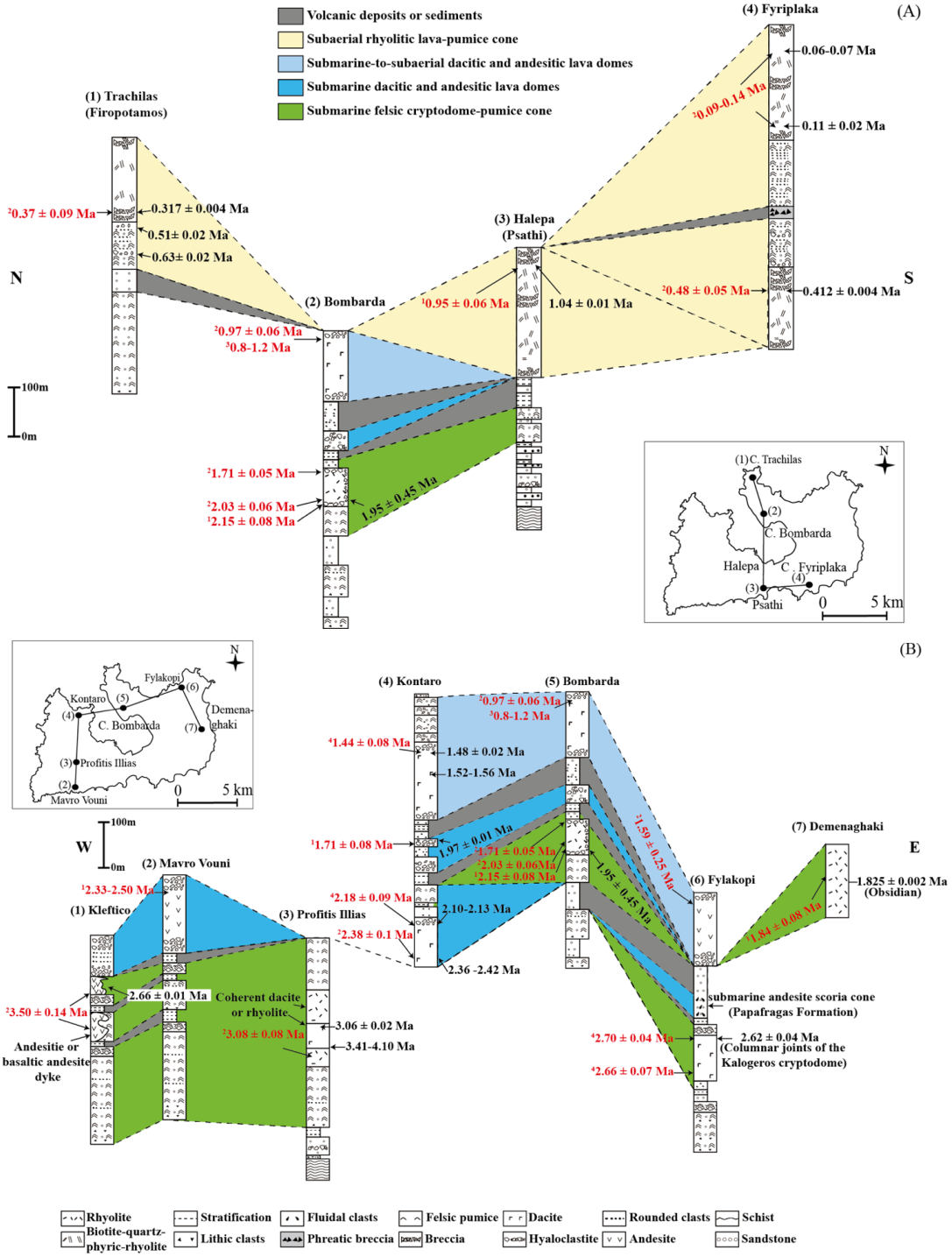

Figure 14. Nine selected stratigraphic columns covering the (A) old (>1.4 Ma) and (B) young (<1.4 Ma) volcanic deposits of Milos modified after Stewart and McPhie (2006). Age data in black are from this study and in red are from: 1=Angelier et al. (1977), 2=Fytikas et al. (1976, 1986), 3=Matsuda et al. (1999), 4=Stewart and McPhie (2006).

https://doi.org/10.5194/gchron-2020-30
Preprint. Discussion started: 13 October 2020

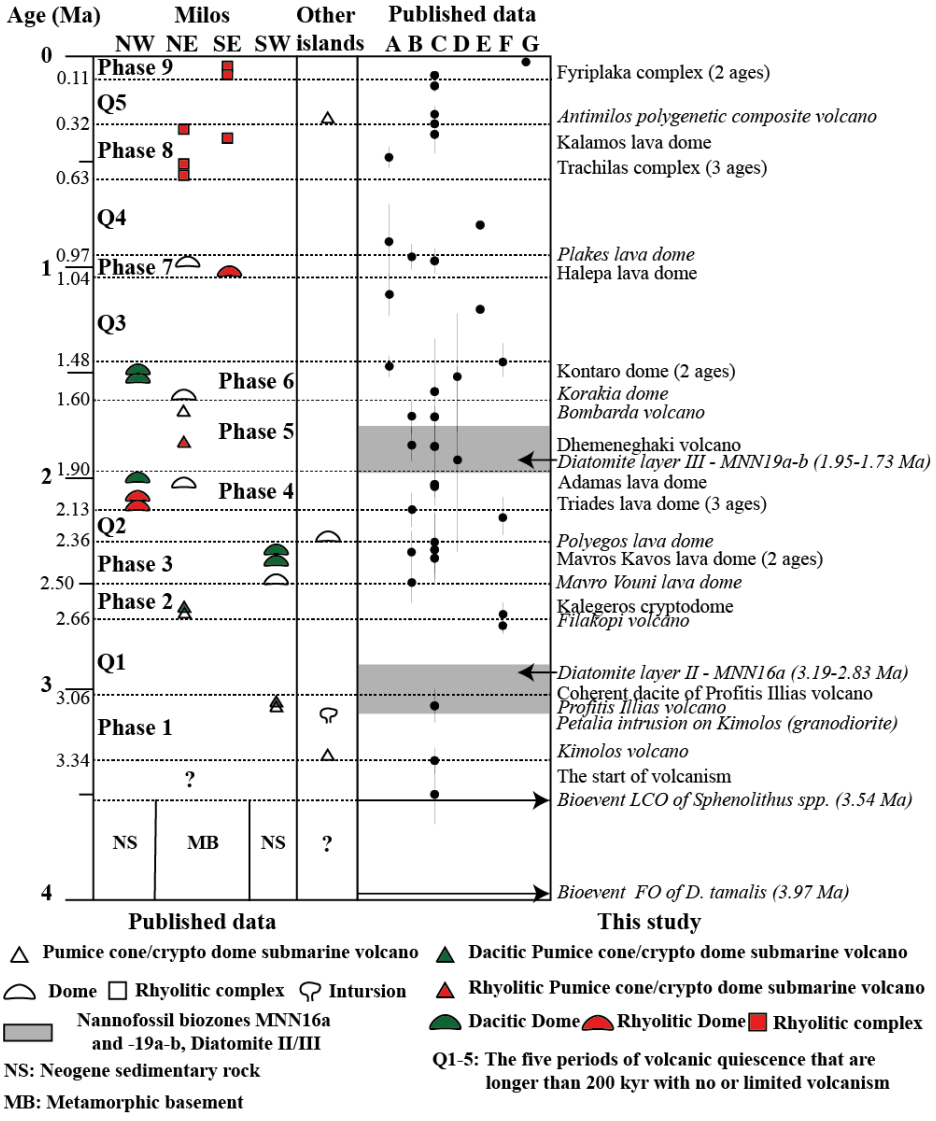

Figure 15. Diagram comparing the proposed nine volcanic phases and four periods of quiescence of Milos based on the new $^{40}Ar/^{39}Ar$ data of this study (indicated by solid symbols) and published age data (indicated by open symbols, names in italic). The volcano types for the different volcanic units (left panel) are from Stewart and McPhie (2006). The location of the different volcanoes is given in Fig 3. and indicated in the left panel (from left to right: NW, NE, SE and SW of Milos). The right panel corresponds to published data: [A]=Fytikas et al., 1976, [B]=Angelier et al., 1977, [C]=Fytikas et al., 1986, [D]= Bigazzi & Radi, 1981, [E]=Matsuda, 1999, [F]=Stewart and McPhie (2006) and [G]=Principle 2002. Biostratigraphic data of the Neogene sediments (NG) is from Van Hinsbergen et al. (2004) calibrated to Gradstein et al. (2012) (LCO of Sphenolithus spp. and FO of D. tamalis) and Calvo et al. (2012). The start of volcanism (3.34-3.54 Ma) on Milos and the basement underneath Kimolos, Polyegos and Antimilos islands is not well constraint and indicated with question marks (see text for discussion).

https://doi.org/10.5194/gchron-2020-30
Preprint. Discussion started: 13 October 2020

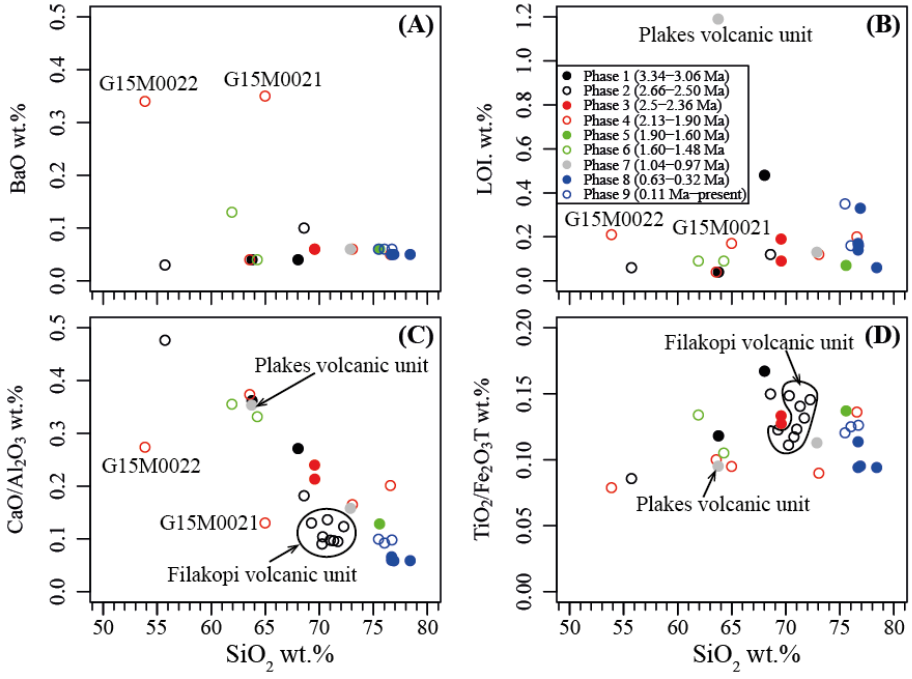

Figure 16. SiO_2 wt.% versus (A) BaO wt.%, LOI. wt.%, (C) CaO/Al_2O_3 and (D) TiO_2/Fe_2O_3T for the nine volcanic phases of the Milos volcanic field. The published data of Filakopi and Plakes volcanic units are from Stewart and McPhie (2003) and Fytikas et al. (1986), respectively.

Supplement (supplements I: field images, II: $^{40}Ar/^{39}Ar$ analytical data and III: X-Ray reports).